International Journal of Nanomedicine

Dovepress
open access to scientific and medical research

Open Access Full Text Article

ORIGINAL RESEARCH

Polyphenol-Conjugated Bimetallic Au@AgNPs for Improved Wound Healing

This article was published in the following Dove Press journal:
International Journal of Nanomedicine

Piotr Orlowski[1]
Magdalena Zmigrodzka[2]
Emilia Tomaszewska[3]
Katarzyna Ranoszek-Soliwoda[3]
Beata Pajak[4]
Anna Slonska[5]
Joanna Cymerys[5]
Grzegorz Celichowski[3]
Jaroslaw Grobelny[3]
Malgorzata Krzyzowska[1]

[1]Laboratory of Nanobiology and Biomaterials, Military Institute of Hygiene and Epidemiology, Warsaw, Poland; [2]Department of Pathology and Veterinary Diagnostics, Institute of Veterinary Medicine, Warsaw University of Life Sciences (WULS-SGGW), Warsaw, Poland; [3]Department of Materials Technology and Chemistry, Faculty of Chemistry, University of Lodz, Lodz, Poland; [4]Laboratory of Genetics and Molecular Biology, Military Institute of Hygiene and Epidemiology, Warsaw, Poland; [5]Division of Microbiology, Department of Preclinical Sciences, Institute of Veterinary Medicine, Warsaw University of Life Sciences, Warsaw 02-786, Poland

Background: Polyphenols possess antioxidant, anti-inflammatory and antimicrobial properties and have been used in the treatment of skin wounds and burns. We previously showed that tannic acid-modified AgNPs sized >26 nm promote wound healing, while tannic acid-modified AgNPs sized 13 nm can elicit strong local inflammatory response. In this study, we tested bimetallic Au@AgNPs sized 30 nm modified with selected flavonoid and non-flavonoid compounds for wound healing applications.

Methods: Bimetallic Au@AgNPs were obtained by growing an Ag layer on AuNPs and further modified with selected polyphenols. After toxicity tests and in vitro scratch assay in HaCaT cells, modified lymph node assay as well as the mouse splint wound model were further used to access the wound healing potential of selected non-toxic modifications.

Results: Tannic acid, gallic acid, polydatin, resveratrol, catechin, epicatechin, epigallocatechin, epicatechin gallate, epigallocatechin gallate and procyanidin B2 used to modify Au@AgNPs exhibited good toxicological profiles in HaCaT cells. Au@AgNPs modified with 15 μM tannic acid, 200 μM resveratrol, 200 μM epicatechin gallate, 1000 μM gallic acid and 200 μM procyanidin B2 induced wound healing in vivo and did not lead to the local irritation or inflammation. Tannic acid-modified Au@AgNPs induced epithelial-to-mesenchymal transition (EMT) – like re-epithelialization, while other polyphenol modifications of Au@AgNPs acted through proliferation and wound closure.

Conclusion: Bimetallic Au@AgNPs can be used as a basis for modification with selected polyphenols for topical uses. In addition, we have demonstrated that particular polyphenols used to modify bimetallic nanoparticles may show different effects upon different stages of wound healing.

Keywords: polyphenols, bimetallic nanoparticles, wound healing, mouse model

Introduction

Polyphenols are a class of naturally occurring compounds having multiple numbers of hydroxyl groups attached to aromatic rings.[1–3] They are synthesized as secondary metabolites and are divided into flavonoid and non-flavonoid compounds. Flavonoids consist of flavonols, flavones, flavanones, flavan-3-ols, isoflavones and anthocyanidins. The non-flavonoid metabolites include phenolic acids, lignans, stilbenes, tannins and lignins.[1–4] Polyphenols exhibit a large and diverse array of biological properties, with a great potential for the treatment of lifestyle-related diseases, such as type 2 diabetes, obesity, and metabolic syndrome.[5,6] They have been also reported to prevent from aging, Alzheimer's disease, cardiovascular diseases, and cancer.[7–9] The most common properties of polyphenols—antioxidant, anti-inflammatory and antimicrobial indicate that they may be used in the treatment of various skin damages, such as wounds and burns.[10,11]

Correspondence: Malgorzata Krzyzowska
Email krzyzowskam@yahoo.com

submit your manuscript | www.dovepress.com
DovePress
http://doi.org/10.2147/IJN.S252027

Wound healing is a process which aims to restore the integrity of the skin as rapidly as possible. It is divided into four stages that overlap in time and space: hemostasis, inflammation, new tissue formation (granulation and angiogenesis) and tissue remodeling. Various cell types such as leukocytes, fibroblasts and keratinocytes, which are controlled by several factors, including cytokines, chemokines, growth factors and enzymes interact with each other at each stage of wound healing.[12,13] Prolonged inflammation delays wound closure. Chronic wounds represent a major health burden and remain a challenging clinical problem.[13,14] Many studies have been focused on wound healing improvement and development of new drugs and/or dressings that promote wound healing.

In our previous papers, we demonstrated that tannic acid-modified AgNPs sized above 30 nm showed a good toxicological profile in human HaCaT and VK2-E6/E7 keratinocyte cell lines and possessed immunomodulatory and antimicrobial properties useful for potential dermal applications.[15] Tannic acid-modified AgNPs sized >30 nm also promoted wound healing in the mouse model.[16]

AuNPs and AgNPs are the most widely used nanomaterials in biomedical applications. AuNPs exhibit chemical stability and biocompatibility, while AgNPs show good antimicrobial effects.[17] However, AgNPs are less stable under identical biological and chemical conditions than AuNPs, and may show toxic effects in biological systems. Therefore, a combination of gold and silver in one bimetallic nanostructure helps to obtain a new set of properties resulting from both metals.

Bimetallic gold-silver nanostructures exhibit unique electronic,[18] optical,[19] and biological properties.[20] Bimetallic core–shell NPs are nanostructures where one metal element forms an inner core and is surrounded by a shell from another metal. Core-shell structures containing both gold and silver material (for example, Au@AgNPs – a gold core and a silver shell) have already been investigated.[19–24] Au@AgNPs were first synthesized by Morriss and Collins[19] for plasmonic applications. Core-shell Au@AgNPs show antibacterial properties and excellent photothermal activity.[22] Antibacterial activity of bimetallic gold and silver NPs was detected against both Gram-negative (*Escherichia coli* and *Pseudomonas aeruginosa*) and Gram-positive (*Enterococcus faecalis* and *Pediococcus acidilactici*) bacteria with more efficacy against Gram-negative bacteria.[20] Au@AgNPs were also used as optical biosensors to detect staphylococcal enterotoxin.[23]

The potential wound healing of bimetallic core–shell NPs still remains unexplored. Taking into account polyphenol usefulness in wound healing, the combined use of bimetallic NPs and polyphenols may create new possible drugs or dressings which can prove new or better properties.

In this paper, Au@AgNPs, sized 30 nm, were modified with different polyphenolic compounds: gallic acid (a building unit of tannic acid), gallic acid derivatives (epicatechin gallate, epigallocatechin gallate), and compared with other compounds containing the epicatechin core: epicatechin and epigallocatechin. The polyphenols were selected based on the analysis of the composition of the green tea extract, which has been known for its bioactive and wound healing properties.[25] As the structural references two more tannins: i) resveratrol and ii) procyanidin B2 were selected. Resveratrol is the smallest polyphenol molecule with a well-known bioactivity[26] in the pure form and as a complex with glucose – polydatin (naturally present in grapes). Both compounds are commercially available both in the pure form and in many extracts. Procyanidin B2 is the most basic example of non-hydrolysable tannins, commercially available in the pure form. This tannin contains two condensed epicatechin derivative substructures similar to those present in the green tea extract.

This paper uses in vitro and in vivo model to test wound healing properties of bimetallic Au@AgNPs modified with different polyphenols.

Materials and Methods

Synthesis of Nanoparticles

Chemicals

All chemical reagents used for the synthesis and functionalization of nanoparticles were purchased from commercial suppliers: gold (III) chloride hydrate ($HAuCl_4 \cdot xH_2O$, Au ≥49, Sigma-Aldrich, Saint Louis, MO, USA), silver nitrate ($AgNO_3$, purity 99.999%, Sigma-Aldrich), sodium citrate dihydrate ($C_6H_5Na_3O_7 \cdot 2H_2O$, ≥99.0%, Sigma-Aldrich), polyphenols (Extrasynthese, Genay, Cedex, France). For all preparations, deionized water was used (Deionizer Millipore Simplicity UV system, specific resistivity of water was equal to 18.2 MΩ·cm).

Nanoparticle Synthesis and Functionalization

Au@AgNPs were prepared by the seeded growth-mediated method. AuNPs with the size of about 13 nm were synthesized in water according to chemical reduction method and used as crystallization seeds for the growth of AgNPs by reduction of Ag^+ ions with sodium citrate. The AuNPs were synthesized by the standard citrate method with $HAuCl_4$ reported in our previous work.[27] Briefly, chloroauric acid aqueous solution (95.4 g, 1.81·10-2% wt.) was heated under reflux with vigorous stirring to the boiling point. Next, a solution of sodium citrate (4.6 g, 1% wt.) was added into the flask and the mixture was heated for additional 15 min and next cooled down to room temperature. The molar ratio of $HAuCl_4$ to sodium citrate was 1:3.5 and the concentration of gold in colloid was 100 ppm.

The synthesis of silver shell on AuNPs seeds (Au@AgNPs) was as follow: 10.3 g of AuNPs seed solution, 37.6 g of deionized water and 6 g sodium citrate solution (1%) were heated to the boiling point under reflux. Next, 6 g of silver nitrate aqueous solution (0.13%) was added to the reaction flask through a capillary tube with syringe pump (the flow rate equal 6 mL h−1; syringe diameter 10 mm). After the addition of all reagents, the mixture was heated for additional 15 min, and next was cooled down to room temperature in the water bath.

Au@AgNPs were functionalized with polyphenols by incubation of aqueous modifier solution at appropriate concentration (15–1000 μm/l). The diagram showing the work-flow is presented in Supplementary Figure 1.

Nanoparticle Characterization Techniques

The hydrodynamic size and colloidal stability of Au@AgNPs before and after polyphenol functionalization were investigated by dynamic light scattering (DLS) measurements (Anton Paar; laser wavelength 658 nm; scattering angle 173°; measurement temperature 25°C; medium viscosity 0.8903 mPa s−1; medium refractive index 1.330; silver refractive index 0.280). All measurements were performed in a quartz microcuvette.

The size of Au@AgNPs was measured with High Resolution-Scanning Transmission Electron Microscopy (HR-STEM, Nova NanoSEM 450, FEI) using the transmission mode (STEM II) at accelerating voltage of 30 kV. Samples for measurements were prepared by placing a drop of colloid onto carbon-coated copper grid and left for 2h for solvent evaporation.

Cell Culture and Toxicity Tests

Human HaCaT keratinocytes were obtained from CLS Cell Lines Service GmbH (Eppelheim, Germany) and propagated in Dulbecco's modified MEM (DMEM) supplemented with 10% fetal calf serum, 10 U/mL penicillin and 100 μg/mL streptomycin (Gibco by Thermo Fisher Scientific, Carlsbad, CA, USA). The cells were seeded into 24 well plates at the density of $5x10^4$/mL cells and cultured for 24 h before exposure to nanoparticles at the concentration range of 0.5–10 μg/mL. After another 24 h cells were used for further analyses.

Toxicity of polyphenol-modified Au@AgNPs was accessed using a cationic dye, 5,5′,6,6′-tetrachloro1,1′,3,3′-tetraethyl-benzimidazolylcarbocyanine iodide (JC-1) (Sigma-Aldrich, Saint Louis, Missouri, USA), as described previously.[15,16] The stained cells were analysed in FACS Calibur using CellQuest program (BD Biosciences, USA).

ROS Production

The ROS generation was determined by a fluorometric assay with 2′,7′-dichlorofluorescein diacetate (DCFH-DA) (Sigma-Aldrich), as described previously.[15,16] The dye-loaded cells were harvested and the fluorescence was measured at 520 nm emission wavelengths in FACS Calibur flow cytometer.

Wound Assay in vitro

HaCat cells were plated in 24-well dishes and cultured to 100% confluence. Scratches were produced using a 200 μL pipette tip, as described by Liang et al[28] and Orlowski et al.[16]

Visualization of Au@AgNPs

For microscopy detection of nanoparticles, cells were grown on coverslips at a density of 1 x 10^5/mL for 18 h before exposure to nanoparticles. After 24h of exposure to 10 μg/mL of Au@AgNPs, the medium was discarded and cells were fixed with 4% paraformaldehyde (PFA) in PBS, washed twice with PBS and covered with PBS containing 2 μg/mL Hoechst 33342 (Sigma-Aldrich). Confocal images were acquired using a Fluoview FV10i laser scanning confocal microscope (Olympus Polska Sp. z o.o.) with a 10x air lens and a 60x water immersion lens, using ultraviolet/visible light LD lasers with excitation at 638 nm. Nanoparticles were visualized in the reflection mode.

Western Blotting

Cells were collected from 6-well dishes and lysed on ice in RIPA buffer (1x PBS, 10 mL/L Igepal CA-630, 5 g/L sodium deoxycholate, 1 g/L SDS, 0.4 mM PMSF, 10 µg/mL of aprotinin and 10 µg/mL of sodium orthovanadate, Sigma Aldrich) for 30 min. After centrifugation (10,000 g, 5 min) whole-cell protein levels were quantified with Bradford assay using solution of commercial Bradford reagent (Bio-Rad) (1:4 v/v) in water. Samples containing equal amounts of protein (20 µg) were separated by SDS-PAGE and transferred to PVDF membranes. After blocking in 5% skimmed milk in TBST (NaCl 137 mM, KCl 2.7 mM, Tris base 19 mM, 0.1% Tween), membranes were probed overnight at 4°C with primary antibodies against: e-cadherin (1:200, mouse, sc-8426, Santa Cruz Biotechnology), PCNA (1:200, mouse, sc-56, Santa Cruz Biotechnology), MMP-9 (1:500, rabbit, ab38898, Abcam), involucrin (1:500, rabbit, ab53112, Abcam) and actin (1:500, goat, sc1516, Santa Cruz Biotechnology). Membranes were then incubated with an HRP conjugated secondary antibody: goat anti-rabbit (Cell Signaling Technology, 7074S) or donkey anti-mouse (Sigma Aldrich) or donkey anti-goat (Sigma Aldrich) for 1 h at room temperature (RT). Chemiluminescence detection of proteins was obtained using ECL (Thermo Fisher Scientific, 32209) and standard x-ray film developing. Subsequent quantification of band images was performed using analysis software – Image Studio Lite Version 5.2.5 (LI-COR Biotechnology – GmbH, Hamburg, Germany).

Ethical Statement

The study was performed in accordance with the recommendations of the Polish Act of 21 January 2005 on animal experiments (OJ no 33, item 289) and Directive 2010/63/EU of the European Parliament and the Council of 22 September 2010 on the protection of animals used for scientific purposes. The protocol was approved by the 4th Local Committee on the Ethics of Animal Experiments in Warsaw, Poland (permit Number: 76/2015 and WAW2/059/2018).

Wound Model in vivo

Female C57BL6 mice (Medical University of Bialystok, Bialystok, Poland), 8 weeks of age, were assigned to groups (5 animals per group). Mice were anesthetized by intraperitoneal injection of 85 mg/kg ketamine (Biowet, Pulawy, Poland) and 10 mg/kg xylazine (Xylopan, Polypharm S.A., Warsaw, Poland). Hair removal and skin wounding were performed as described previously.[16] Modified Au@AgNPs nanoparticles or corresponding polyphenol solutions were applied at 5 µg/mL in saline in the volume of 100 µL to one wound, and a vehicle control to the other. The wound was covered with a transparent occlusive dressing (3M Health Care, Neuss, Germany). 5 mg/kg of meloxicam (Loxicom, ScanVet, Gniezno, Poland) was administered once daily via subcutaneous injection for the post-operative pain relief during first 3 days. At 3, 6 and 14 days, mice were given euthanasia, wounds were excised and used for further tests.

Morphological Analysis of Wound Re-Epithelialization and Inflammatory Infiltration

Skin specimens were fixed in 4% paraformaldehyde buffered with PBS (pH 7.4) and embedded in paraffin. Tissue sections were stained with hematoxylin/eosin and Gomori's Trichome Special Stain Kit according to the manufacturer's instructions (Leica Biosystems, Kawaska, Zalesie, Poland). The images were captured with the Zeiss Axio Imager.M2 (Zeiss GmbH, Oberkochen, Germany). Wounds were assessed as described previously,[16] ie the wound closure was calculated as the percentage of wound area at the time point in comparison to the initial wound area. The epithelial sheet area (re-epithelialization) was measured in the cross-sections stained with hematoxylin/eosin using ZEN software. Neutrophils were counted in five randomly selected microscope fields per section in the wound cavity at 400-fold magnification (0.234 mm^2).

Local Lymph Node Assay (LLNA)

Female BALB/c mice (Medical University of Bialystok, Bialystok, Poland), 8 weeks of age, were assigned to groups (3 animals per group) using a stratified random grouping method based on individual body weights. Ears were stripped 10 times with an ordinary adhesive tape (Polopor, Viscoplast, Polfa Warszawa, Poland), as described before.[16] After tape stripping, a vehicle negative control (acetone: olive oil, 3:1), a positive control – 25% w/v citral in vehicle (Sigma-Aldrich) and 25% w/v of polyphenol-modified Au@AgNPs in vehicle or corresponding tannin solution in vehicle were applied to the dorsum of each ear (25 µL/ear) once daily for three consecutive days. To access lymphocyte proliferation in auricular lymph nodes, Cell Proliferation ELISA,

BrdU colorimetric kit (Sigma-Aldrich) was used. Shortly, cells were seeded in 96-well round bottom plates at 10^4 cells per well in RPMI medium without phenol red supplemented with 10% FBS, 10 U/mL penicillin, 100 µg/mL streptomycin (Gibco), 2 µg/mL concanavalin A (Sigma-Aldrich) and at 72h, BrdU was added and the cells were incubated for another 24h. BrdU incorporation was further detected according to the manufacturer's protocol. The absorbance was measured using FLUOstar Omega counter (BMG Labtech, Ortenberg, Germany).

Quantitative Reverse Transcriptase-Polymerase Chain Reaction (RT2-PCR)

Total RNA was isolated from the wound tissues preserved in RNAlater (Sigma Aldrich) using Universal RNA Purification Kit (EURx, Gdansk, Poland). Transcripts of TNF-α, VEGF-α, PDGF-β, IL-1α and TGF-β1 were quantified using Taqman Gene Expression Assays (Thermo Fisher Scientific). All PCR reactions were carried out with QuantiFast Probe RT-PCR Kit (Qiagen, Hilden, Germany) using a real-time PCR instrument Stratagene MX4000 Real-Time qPCR System (Agilent Technologies) according to the manufacturer's protocol. The 2-ΔΔCt method was used in calculating the relative ratio to control uninfected tissue.

Statistical Methods

Data are shown as the mean ± standard error of the mean (SEM) from at least three independent experiments. Data were analysed using a two-tailed paired Student's *t*-test (normal distribution) or with non-parametric Kruskal–Wallis and Wilcoxon's tests were applied using Biostat software (AnalystSoft Inc., CA, USA). In every analysis values of $p \leq 0.05$ were considered significant.

Results

Characterisation of Au@AgNPs Modified with Polyphenols

Figure 1A represents the schematic illustration of the Au@AgNPs core-shell structure used for further functionalization and biological experiments. The Au@AgNPs were designed as spherical silver nanoparticles with the size equal to 30 nm containing gold core with the size equal to 13 nm. To confirm the core-shell structure of nanoparticles, Au@AgNPs were tested with the high-resolution scanning transmission electron microscopy (HR-STEM). The bright-field (BF), dark-field (DF) and high angle annular dark-field (HAADF) detectors were used. The BF detector in HR-STEM is located within the cone of illumination of the transmitted beam and it allows to obtain high-quality morphological images (Figure 1B) while the *DF* detects the scattered electrons which lie outside of the path of the directly transmitted beam (Figure 1C). The most informative for the core-shell structures is the HAADF detector, detecting incoherently scattered electrons and allowing to obtain a Z-contrast image. The Z-image is directly related to the atomic number, hence, it is useful for determination of not only the size and shape of the core-shell structure but it also helps to distinguish two types of materials with different atomic numbers. The high resolution of HAADF gives an advantage over the detection of back scattered electrons (BSE), which can also be used to detect materials with different atomic number, but with a lower resolution for core-shell nanoparticles. The HR-STEM images of synthesized Au@AgNPs core-shell structures are presented in Figure 1B–D.

The HR-STEM revealed that Au@AgNPs are uniform with spherical shape and the mean size is 30 nm. Furthermore, HR-STEM images confirmed the core-shell structure of Au@AgNPs. Based on the image contrast, a silver shell around the gold core can be observed. AuNPs used as seeds for the growth of AgNPs are clearly visible inside the nanoparticles structure as darker areas while the silver shell is visible as a lighter coating. A silver shell of the thickness approx. 8 nm is apparent in the STEM images (Figure 1B–D). In HAADF image of Au@AgNPs (Figure 1D) the AuNPs seeds are seen as white structures. It is known that HAADF images are formed by collection of only very high angle, incoherently scattered electrons. As a result, HAADF detector is highly sensitive to atomic number of atoms present in the material (Z-contrast). For elements with a larger atomic number, the electrostatic interactions between the nucleus and the electron beam are higher, hence more electrons are scattered at higher angles. As a result, the HAADF detects more signals from atoms with higher atomic number and these elements can be seen as brighter areas in the resulting image – AuNPs seeds with ZAu = 79, while the Ag shell (ZAg = 47) on the same image is seen as darker areas (Figure 1D).

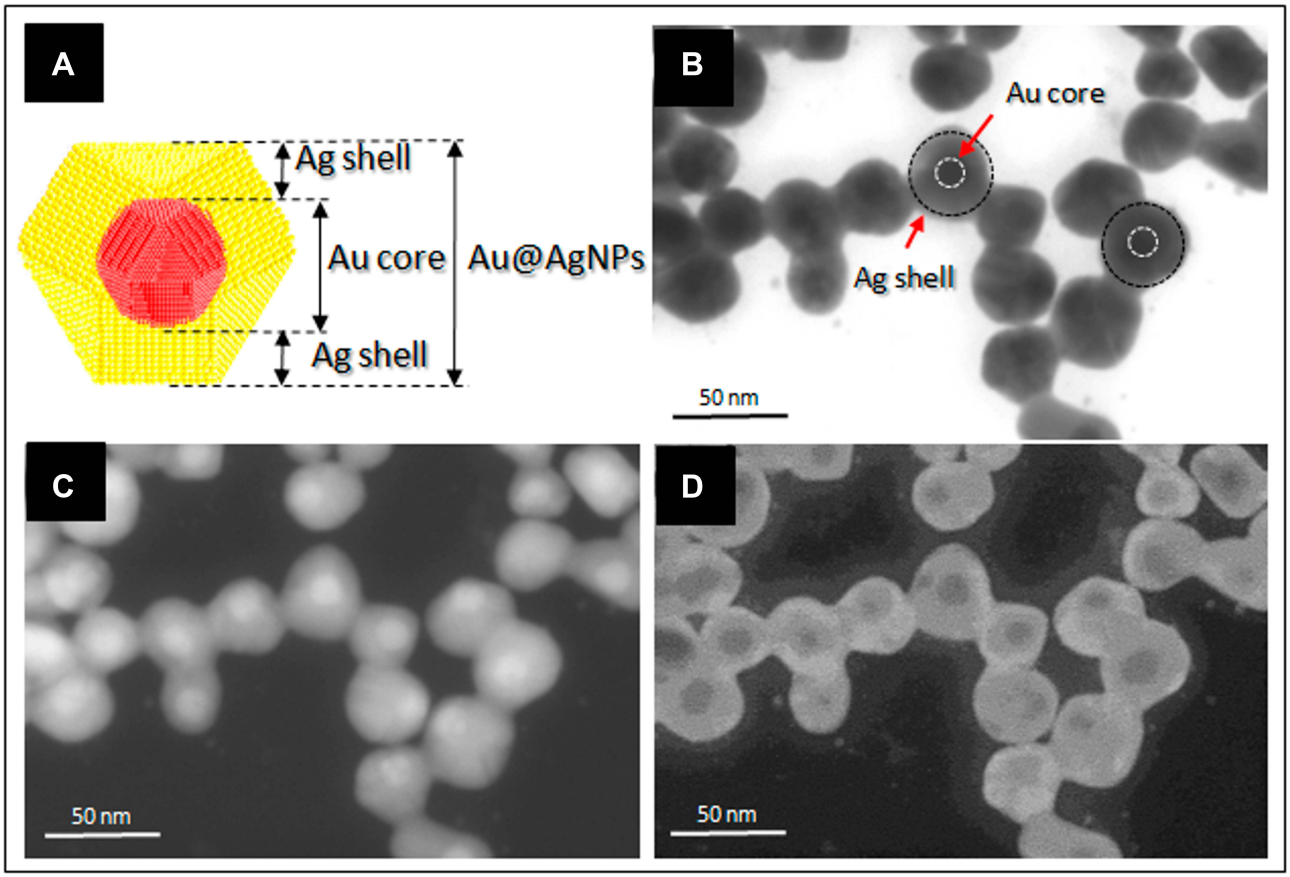

Figure 1 Schematic representation of the Au@AgNPs synthesis strategy (**A**) and HR-STEM images of synthesized Au@AgNPs (**B**–**D**) bright field (**B**); dark field (**C**); and high angle annular dark field (**D**).

The hydrodynamic size and the colloidal stability of Au@AgNPs were investigated with DLS measurements. The DLS size distribution histogram is presented in Figure 2A. The mean hydrodynamic size of citrate Au@AgNPs is equal to 33 nm. Colloid was stable and any aggregates were not observed. Au@AgNPs were functionalized with different polyphenols and characterized by DLS technique. The DLS size distribution histograms of Au@AgNPs after functionalization with gallic acid (GAL), resveratrol (RES), epigallocatechin gallate (EGC), procyanidin B2 (PRO) and tannic acid (TAN) are presented in Figure 2B–F.

All Au@AgNPs colloids were stable after functionalization. The mean size of hydrodynamic diameter increased after the Au@AgNPs modification and was: 36 nm, 45 nm, 61 nm, 63 nm and 38 nm for GAL-Au@AgNPs, RES-Au@AgNPs, EGC-Au@AgNPs, PRO-Au@AgNPs and TAN-Au@AgNPs, respectively. The increase of the hydrodynamic size of particles results from the size of the modifier molecule, ie, the larger the modifier molecule, the larger is the hydrodynamic diameter of the nanoparticle. Such a relationship was not observed for TAN-Au@AgNPs because the amount of TAN used to modify was much smaller compared to other polyphenols (15 µmol/l for tannic acid, 1000 µmol/l for gallic acid; 200 µmol/l for resveratrol, epigallocatechin gallate, procyanidin B2).

Toxicity of Au@AgNPs Modified with Polyphenols in vitro

At 24h of incubation with Au@AgNPs, the mitochondrial potential ($\Delta\Psi m$) was measured using the JC-1 assay. As shown in Table 1, the cytotoxic effect of Au@AgNPs modified with polyphenols upon the mitochondrial potential was minimal, except for modification with (15–340 µM) tannic acid and 200 µM epigallocatechin gallate ($p \leq 0.05$) (Table 1). All corresponding polyphenol solutions did not induce any toxicity, except for 340 µM tannic acid causing mitochondrial toxicity already at 5 µg/mL ($p \leq 0.05$)

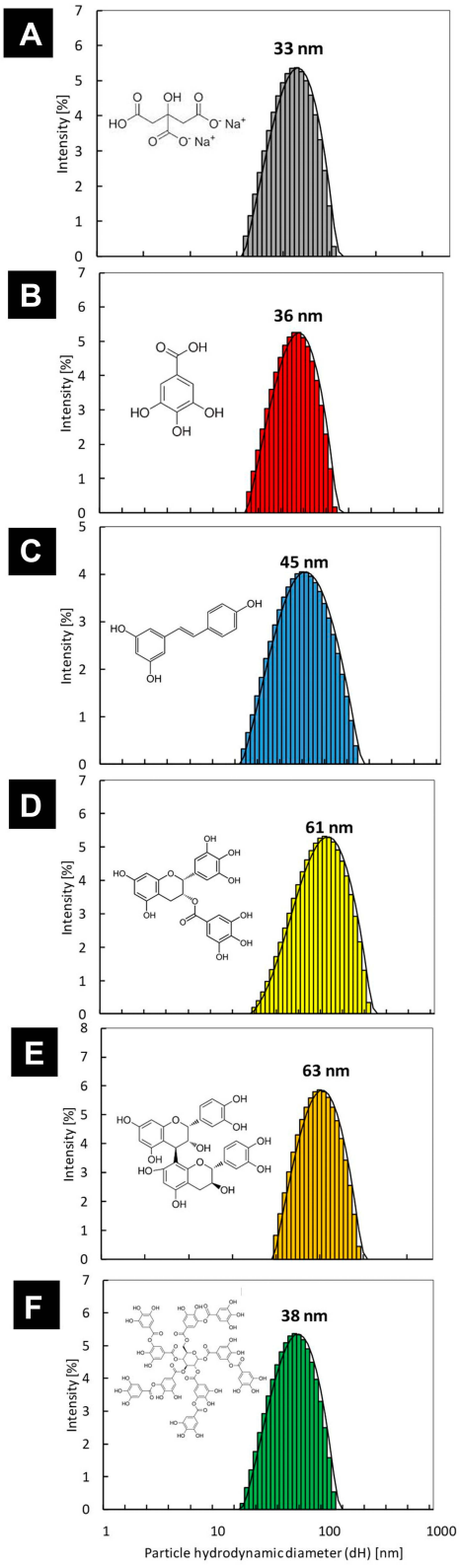

Figure 2 The DLS size distribution histograms with the mean hydrodynamic size of nanoparticles: citrate Au@AgNPs (**A**), GAL-Au@AgNPs (**B**); RES-Au@AgNPs (**C**); EGC-Au@AgNPs (**D**); PRO-Au@AgNPs (**E**); TAN-Au@AgNPs (**F**) with the respective chemical structure of compounds used for the functionalization.
Abbreviations: ECG, epicatechin gallate modified; GAL, gallic acid modified; PRO, procyanidin B2 modified; RES, resveratrol modified; TAN, tannic acid modified.

(Table 1). Au@AgNPs modified with 200 μM epigallocatechin gallate significantly decreased mitochondrial potential at 10 μg/mL, in comparison to 200 μM epigallocatechin gallate reference solution ($p \leq 0.05$) (Table 1), while 100 μM epigallocatechin gallate had no significant toxic effects (Table 1).

We previously showed that tannic acid-modified AgNPs sized 13 and 33 nm induced production of reactive oxygen species in HaCaT cells.[15] The concentration of the tannic acid used in this work was 340 μM. Here, we used lower concentrations for modifications, such as 15 and 170 μM to found that the latter actually significantly decreased ROS production by HaCaT cells, when used at 5 μg/mL ($p \leq 0.05$) (Table 2). Also, polydatin, resveratrol and epicatechin reduced production of ROS in a concentration-dependent manner ($p \leq 0.05$) (Table 2). On the other hand, 340 μM of tannic acid and 100 μM epigallocatechin significantly increased ROS production ($p \leq 0.05$) (Table 2).

Wound Healing Potential Depends on the Type and Concentration of a Polyphenol Used for Modification of Au@AgNPs

Next, we decided to find if modification of bimetallic nanoparticles with polyphenols leads to an additive effect on the migration of keratinocytes in cell culture. The scratch assay using human HaCaT cell line is a well-characterized method to measure keratinocyte migration in vitro.[28] The scratch area of HaCaT cells treated with modified bimetallic nanoparticles at 5 μg/mL or with a corresponding concentration of a polyphenol used for modification appeared to have a greater number of keratinocytes present within the scratch region when compared to control cells (Figure 3) but also to cells treated with unmodified Au@AgNPs ($p \leq 0.05$) (Figure 3). For tannic acid (TAN), the migration of keratinocytes was inversely proportional to its concentration used for modification, with the Au@AgNPs-15 μM TAN conjugate showing significantly higher migration of keratinocytes in comparison to the polyphenol solution ($p \leq 0.01$) (Figure 3A). However, only TAN-modified Au@AgNPs showed a significant increase of cell migration ($p \leq 0.05$) (Figure 2A).

Gallic acid (GAL), a structural unit of gallotannins such as tannic acid, significantly better induced cell migration when used for Au@AgNPs modification in comparison to its solution ($p \leq 0.01$) (Figure 3A). This

Table 1 Cytotoxicity of Polyphenol-Conjugated Au@AgNPs in Human HaCaT Keratinocytes. HaCaT Cell Line Was Exposed to Polyphenol-Conjugated Au@AgNPs at 2.5–10 μg/Ml for 24 h and Subjected to Measurement of Mitochondrial Potential with JC-1. TheResults are Expressed as the Percentage of Cells with Decreased Mitochondrial Potential from 3 Separate Experiments ± SEM

Type and Concentration of Polyphenol	Concentration of Polyphenol-Au@AgNP Colloids			Concentration of Polyphenol Solutions		
	2.5 μg/mL	5 μg/mL	10 μg/mL	2.5 μg/mL	5 μg/mL	10 μg/mL
Au@AgNPs without a polyphenol	6.14 ± 2.2	9.94 ± 2.6	9.01 ± 1.1	–	–	–
Tannic acid 15 μM	11.83 ± 3.3	16.79 ± 2.1	26.29 ± 1.5**	5.45 ± 1.4	8.09 ± 3.7	6.72 ± 1.3
Tannic acid 170 μM	9.18 ± 3.2	16.57 ± 2.2	28.91 ± 3.3**	7.3 ± 1.2	7.89 ± 1.4	12.13 ± 1.5
Tannic acid 340 μM	15.32 ± 5.2	22.09 ± 3.4**	44.39 ± 2.3**	14.89 ± 0.9	23.07 ± 2.8**	37.75 ± 4.8 **
Gallic acid 500 μM	6.55 ± 2.1	8.39 ± 1.8	8.41 ± 1.5	7.02 ± 0.9	6.31 ± 1.6	8.22 ± 2.3
Gallic acid 1000 μM	9.03 ± 1.7	13.3 ± 2.9	14.9 ± 3.0	7.11 ± 1.4	6.04 ± 2.0	5.96 ± 0.9
Polydatin 200 μM	10.09 ± 1.7	9.31 ± 1.15	15.4 ± 1.6	8.55 ± 0.9	9.53 ± 1.3	10.61 ± 0.8
Resveratrol 200 μM	7.6 ± 0.31	7.78 ± 0.13	12.94 ± 1.2	6.23 ± 1.4	6.25 ± 1.4	5.38 ± 0.6
Catechin 200 μM	11.26 ± 1.5	17.1 ± 0.9	19.14 ± 1.5	6.12 ± 0.8	8.45 ± 0.9	10.5 ± 1.52
Epicatechin 100 μM	10.01 ± 1.8	12.17 ± 1.4	13.18 ± 2.1	8.09 ± 2.5	12.65 ± 1.5	12.45 ± 1.3
Epicatechin 200 μM	11.21 ± 1.8	11.86 ± 1.5	15.88 ± 0.8	8.22 ± 1.5	9.82 ± 1.8	10.83 ± 2.9
Epicatechin gallate 100 μM	5.28 ± 0.6	5.01 ± 0.7	5.99 ± 1.6	4.85 ± 0.5	5.13 ± 0.3	5.2 ± 0.6
Epicatechin gallate 200 μM	5.75 ± 0.6	12.71 ± 3.2	8.47 ± 1.3	5.19 ± 0.3	7.02 ± 0.5	5.36 ± 0.9
Epigallocatechin 100 μM	11.86 ± 5.1	13.32 ± 3.6	15.35 ± 1.5	6.1 ± 0.9	6.03 ± 1.25	7.97 ± 1.0
Epigallocatechin 200 μM	10.55 ± 2.0	10.84 ± 1.6	11.78 ± 0.8	6.01 ± 1.2	7.41 ± 1.1	8.66 ± 0.8
Epigallocatechin gallate 100 μM	5.5 ± 2.2	6.13 ± 1.6	9.86 ± 1.1	5.94 ± 1.2	5.84 ± 1.1	7.26 ± 1.6
Epigallocatechin gallate 200 μM	5.8 ± 0.4	5.27 ± 0.7	18.81 ± 0.7*	4.54 ± 1.0	9.2 ± 1.2	6.19 ± 1.3
Procyanidin 100 μM	10.32 ± 2.3	11.17 ± 1.9	12.61 ± 1.9	12.39 ± 1.1	10.36 ± 2.5	9.15 ± 1.5
Procyanidin 200 μM	11.3 ± 1.9	10.31 ± 2.4	11.87 ± 2.3	6.93 ± 2.1	6.71 ± 1.7	6.42 ± 1.7

Notes: *Represents significant differences with $p \leq 0.05$, while **$p \leq 0.01$.
Abbreviation: SEM, standard error mean.

effect was concentration-dependent, with Au@AgNPs-1000 μM GAL conjugate inducing the highest cell migration (Figure 3A).

Modification of Au@AgNPs with resveratrol or its glucoside form – polydatin showed that modifications with those two stilbenoids induced significantly higher migration of keratinocytes in comparison to unmodified Au@AgNPs ($p \leq 0.05$) (Figure 3B). However, only modification with resveratrol (RES) at 200 μM led to a significant additive effect in comparison to resveratrol solution at the same concentration ($p = 0.01$) (Figure 3B).

Next, we tested modification of Au@AgNPs with flavan-3-ols for stimulation of keratinocyte migration. We found that while epicatechin at 50 and 100 μM significantly increased cell migration ($p \leq 0.05$) (Figure 3C), only modification of Au@AgNPs with 100 μM epicatechin (EPI) led to a significantly increased keratinocyte migration in comparison to unmodified Au@AgNPs ($p = 0.03$) (Figure 3C). On the other hand, modification of Au@AgNPs with its optical isomer, catechin (CAT) at 200 μM induced scratch healing in contrast to the catechin solution itself, although insignificant ($p > 0.05$) (Figure 3C). Epigallocatechin (EGC) as well as its gallate ester, epigallocatechin gallate (EGCG)

Table 2 ROS Production by HaCaT Cell Exposed to Polyphenol-Modified Au@AgNPs. HaCaT Cell Line Was Exposed to Polyphenol-Conjugated Au@AgNPs at 5 and 10 µg/Ml for 24 h and Subjected to ROS Measurement (Materials and Methods). The Results are Expressed as the Mean Green Fluorescence from 3 Experiments ± SEM

Type and Concentration of Polyphenol	Concentration of Polyphenol-Modified Au@AgNPs Colloids	
	5 µg/mL	10 µg/mL
Control cells	274.18 ± 28	
Au@AgNPs without a polyphenol	265.27 ± 23	278.08 ± 16
Tannic acid 15 µM	199.95 ± 21**	286.13 ± 18
Tannic acid 170 µM	246.12± 23	277.09 ± 3.3
Tannic acid 340 µM	245.56± 36*	408.76 ± 7**
Gallic acid 500 µM	342.92 ± 64	371.98 ± 57
Gallic acid 1000 µM	335.88 ± 53	349.95 ± 81
Polydatin 200 µM	197.70 ± 19**	207.67 ± 9*
Resveratrol 200 µM	274.95 ± 20**	199,67 ± 9*
Catechin 200 µM	327.88 ± 41	261.18 ± 12
Epicatechin 100 µM	299.19 ± 51	245.24 ± 28**
Epicatechin 200 µM	245.57 ± 56*	189.31 ± 44*
Epicatechin galate 100 µM	320.99 ± 63	344.46 ± 57
Epicatechin galate 200 µM	357.6 ± 74	373.22 ± 84
Epigallocatechin 100 µM	445.79 ± 40*	298.2 ± 86
Epigallocatechin 200 µM	326.41 ± 35	253.2 ± 25
Epigallocatechin galate 200 µM	346.41 ± 36	377.29 ± 61
Procyjanidin 200 µM	327.29 ± 54	371.2 ± 84

Note: *Represents significant differences with $p \leq 0.05$, while **means $p \leq 0.01$.
Abbreviations: ROS, reactive oxygen species, S.E.M., standard error of mean.

induced significant cell migration leading to a scratch closing ($p \leq 0.05$) (Figure 3C), but when used to modify Au@AgNPs, they did not produce any additive effect upon healing in comparison to Au@AgNPs ($p > 0.05$) (Figure 3C). However, the gallate ester of epicatechin (ECG) used to modify Au@AgNPs at 200 µM induced a significant additive effect upon cell migration ($p = 0.001$) (Figure 3C). Procyanidin B2 (PRO), a natural oligomer of epicatechin showed a significant additive effect upon cell migration within the scratch when used to modify Au@AgNPs at 200 µM in comparison to unmodified Au@AgNPs and procyanidin B2 itself ($p \leq 0.05$) (Figure 3C). Therefore, we decided to use Au@AgNPs modified with 1000 µM gallic acid (GAL), 15 µM tannic acid (TAN), 200 µM resveratrol (RES), 200 µM procyanidin B2 (PRO) and 200 µM epicatechin gallate (ECG) for further tests. Figure 4 shows representative images of HaCaT keratinocytes with internalised nanoparticles (turquoise). We observed no differences in the levels of internalised modified nanoparticles and in general, HaCaT cells showed very low uptake of nanoparticles (Figure 4). Supplementary Figure 1 shows the work-flow for polyphenol modification choice and further tests.

Polyphenol-Modified Au@AgNPs Differently Influence Proliferation and Re-Epithelization by Keratinocytes in vitro

To test the direct effects of polyphenol-modified Au@AgNPs upon keratinocyte biology we first tested the

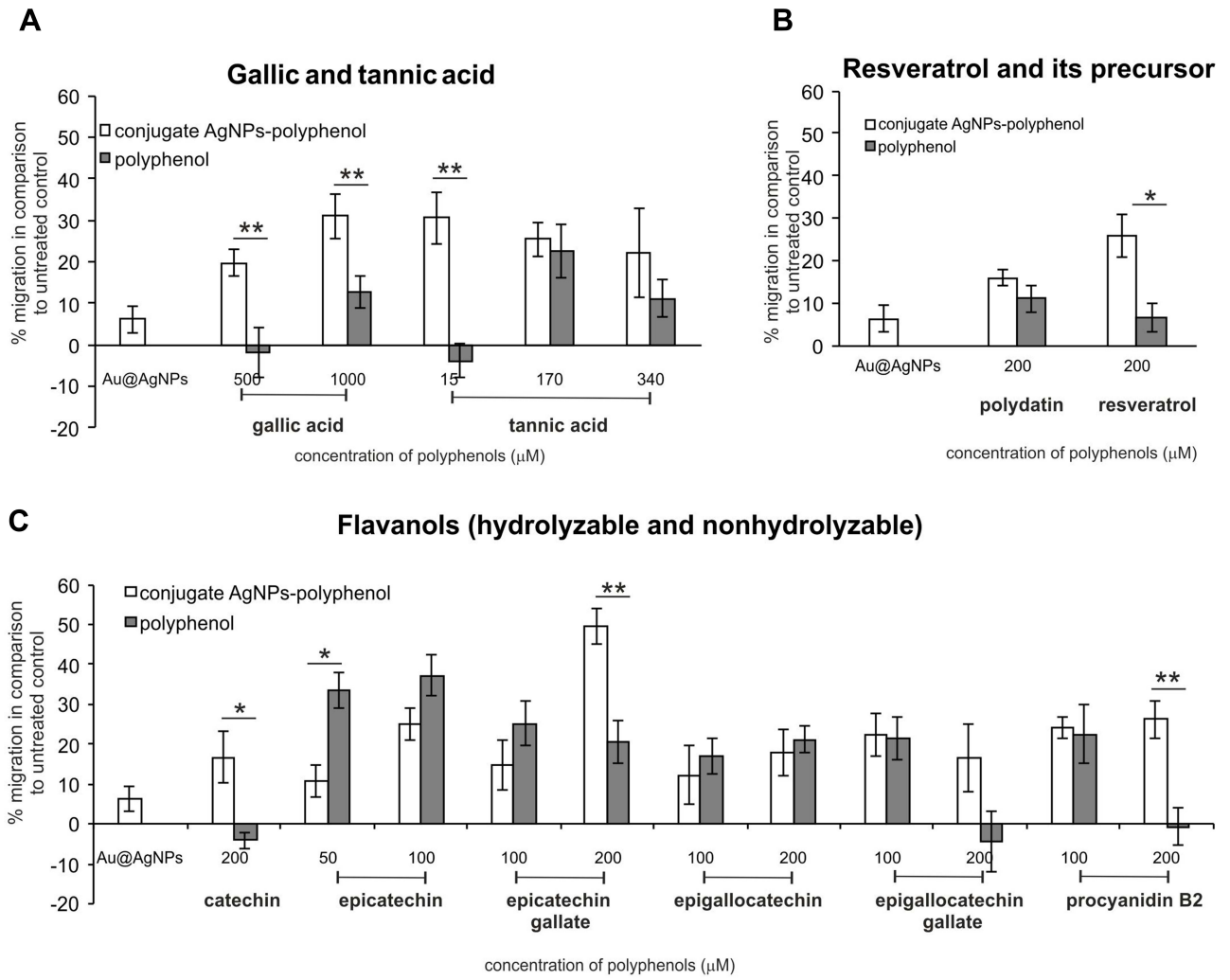

Figure 3 Keratinocyte migration in response to polyphenol-modified Au@AgNPs. Quantitative analysis of scratch assay in HaCaT cell line exposed to citrate-Au@AgNPs, and Au@AgNPs modified with different concentrations of (**A**) tannic acid and gallic acid; (**B**) resveratrol and its precursor, polydatin and (**C**) hydrolysable and nonhydrolyzable flavanols at 5 μg/mL for 24 h. Migration of cells is expressed as % increase in relation to control, unexposed culture with scratch. Each bar represents the mean from 5 experiments (N = 5) ± S.E.M., *represents significant differences with $p \leq 0.05$, while **$p \leq 0.01$.
Abbreviations: S.E.M., standard error of mean.

expression of the proliferation marker, PCNA in HaCaT cells. We found that all tested polyphenols, either alone or in conjugation with Au@AgNPs induced significantly higher proliferation of HaCaT cells ($p \leq 0.05$) (Figure 5, Table 3), except for unmodified Au@AgNPs, tannic acid or TAN-Au @AgNPs-treated cultures ($p > 0.05$) (Figure 5, Table 3).

In comparison to untreated control and cells treated with unmodified Au@AgNPs, TAN-Au@AgNPs as well as with tannic acid itself, all other modified nanoparticles and corresponding polyphenol solutions significantly up-regulated expressions of E-cadherin (120 kDa) ($p \leq 0.05$) (Figure 5, Table 3), while down-regulated production of soluble E-cadherin form (80 kDa) ($p \leq 0.05$) (Figure 5, Table 3). Interestingly, polyphenol-Au@AgNPs conjugates showed lower up-regulation of E-cadherin expression in comparison to corresponding polyphenol solutions (Figure 5, Table 3). Although high expression of E-cadherin is related to keratinocyte differentiation, the process characteristic for the end stage of wound healing, only epicatechin gallate, but not ECG-Au@AgNPs, caused significant up-regulation of involucrin, another marker of keratinocyte differentiation ($p = 0.01$, Figure 5). Matrix metalloproteinase-9 (MMP-9) is a type IV collagenase that is transiently expressed in the process of normal wound healing. Here, we found that Au@AgNPs modified with

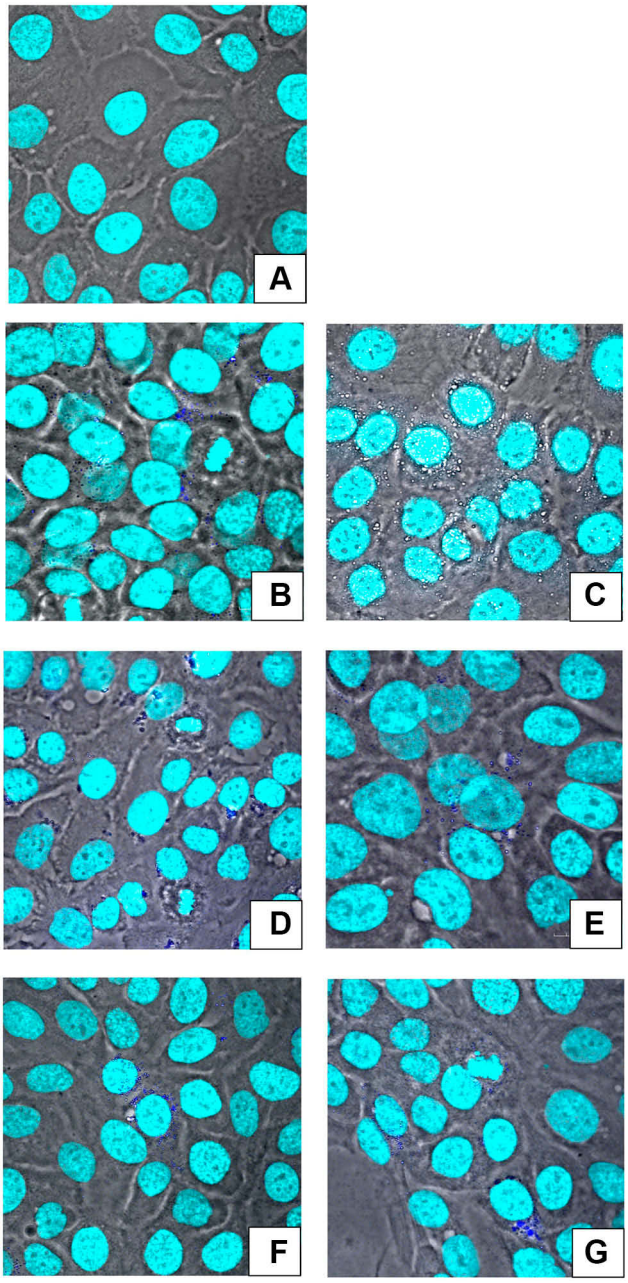

Figure 4 Keratinocytes do not significantly internalize polyphenol-modified Au@AgNPs. Confocal microscopy images showing polyphenol modified and unmodified Au@AgNPs inside the cells (dark blue). (**A**) control, untreated cells, cells treated at 5 μg/mL with (**B**) citrate Au@AgNPs, (**C**) GAL-Au@AgNPs, (**D**) TAN-Au@AgNPs, (**E**) ECG-Au@AgNPs, (**F**) RES-Au@AgNPs and (**G**) PRO-Au @AgNPs, Nuclei were stained with Hoechst 33342 (turquoise). Images were captured using 63 x objective lens and 1.5 x digital zoom.

Abbreviations: TAN, tannic acid modified; GAL, gallic acid modified; ECG, epicatechin gallate modified; RES, resveratrol modified; PRO, procyanidin B2 modified.

gallic acid (GAL), procyanidin B2 (PRO), epicatechin gallate (ECG) and resveratrol (RES) or corresponding polyphenol solutions (except for resveratrol) significantly up-regulated expression of MMP-9 ($p \leq 0.05$) (Figure 5). Unmodified Au@AgNPs down-regulated expression of MMP-9 ($p = 0.01$, Figure 5), while TAN-Au@AgNPs and tannic acid had no significant influence upon MMP-9 expression ($p \geq 0.05$) (Figure 5).

Tannin-Ag/AuNP Conjugates Improve Wound Healing in vivo

Wound closure was observed in all treatment groups within 14 days, albeit with different characteristics (Figure 6). All tested animals formed scabs at the wound site, which lasted for several days and left residual lesions on the skin tissue after they fell off. All tested polyphenol conjugates with Au@AgNPs showed significantly better wound closure at day 6 in comparison to untreated control and unmodified Au@AgNPs ($p \leq 0.05$) (Figures 6A and 7). However, the highest increase in thickness was observed at day 6 for ECG-Au@AgNPs ($p \leq 0.05$) (Figures 6B and 7). The corresponding polyphenol solutions did not significantly influence epithelial thickness at day 6 (Figures 6B and 7). The Au@AgNPs, tannic acid, resveratrol and epigallocatechin gallate-treated wounds showed significantly lower epithelial sheet thickness at day 14 ($p \leq 0.05$) (Figures 6B and 7), while all conjugates showed similar thickness as control wounds, or higher (Figures 6B and 7). For ECG-Au@AgNPs-treated wounds, significantly higher epithelial sheet thickness was observed already at day 3 and 6, in comparison to wounds treated with unmodified Au@AgNPs ($p \leq 0.05$) (Figure 6B). Similarly, wounds treated with TAN-Au@AgNPs showed earlier increase in re-epithelialization at day 6 in comparison to control and Au@AgNPs treatment ($p \leq 0.05$) (Figure 6B). Epithelial sheet thickness observed at day 6 and 14 for GAL-, RES- and PRO-Au@AgNPs were significantly higher than that measured in wounds treated with unmodified Au@AgNPs ($p \leq 0.05$) (Figure 6B). However, these measurements did not differ from those performed for control, untreated wounds (Figure 6B).

Figure 7 shows the wound healing histology for each treatment group at day 6, and 14 after wounding, stained with Masson's trichrome procedure. This staining shows stained collagen fibers in pale blue, the cytoplasm in pale purple, the nuclei in blue, and the red blood cells in cherry red. At the early stage of the healing processes (day 6), wounds in all groups displayed evident inflammatory cell infiltration, granulation tissue formation, and epidermal proliferation. However, wounds treated with polyphenol Au@AgNPs conjugates showed stronger and early collagen deposition and wound closure in comparison to control and Au@AgNPs-treated group (Figure 7).

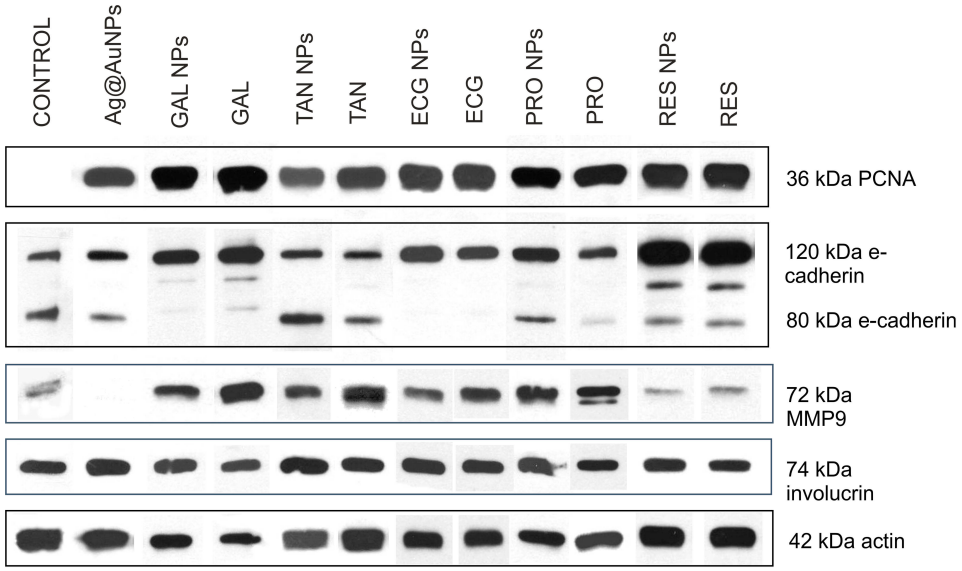

Figure 5 Representative immunoblotting results of involucrin, E-cadherin (80 and 120 kDa), PCNA and MMP-9 in HaCaT cells treated with unmodified and polyphenol-modified Au@AgNPs. Cells were treated at 5 μg/mL with citrate, unmodified Au@AgNPs, GAL-Au@AgNPs, TAN-Au@AgNPs, ECG-Au@AgNPs, RES-Au@AgNPs and PRO-Au@AgNPs for 24h and subjected to Western blotting assay.
Abbreviations: ECG, epicatechin gallate modified; GAL, gallic acid modified; PRO, procyanidin B2 modified; RES, resveratrol modified; TAN, tannic acid modified; PCNA, proliferating cell nuclear antigen; MMP-9, matrix metalloproteinase 9.

To evaluate inflammation in wounds, we calculated the numbers of neutrophils per field (Figure 6C, Supplementary Figure 2). At day 3, we did not find any significant differences in neutrophil infiltration in comparison to control group. Interestingly, starting at day 6 neutrophil infiltration increased significantly for TAN-Au@AgNPs-treated wounds

Table 3 Quantitative Immunoblotting Results of Involucrin, E-Cadherin (80 and 120 kDa), PCNA and MMP-9 in HaCaT Cells Treated with Unmodified and Polyphenol-Modified Au@AgNPs. Cells Were Treated at 5 μg/Ml with Citrate, Unmodified Au@AgNPs, GAL-Au@AgNPs, TAN-Au@AgNPs, ECG-Au@AgNPs, RES-Au@AgNPs and PRO-Au@AgNPs for 24h and Subjected to Western Blotting Assay. The Results are Expressed as Density Measurements from 3 Experiments ± SEM

	PCNA	E-Cadherin 120	E-Cadherin 80 kDa	Involucrin	MMP-9
Control	0.38 ± 065	0.31 ± 0.051	0.23 ± 0.038	0.52 ± 0.1	0.29 ± 0.05
Ag@AuNPs	0.41 ± 0.046	0.35 ± 0.064	0.31 ± 0.09	0.68 ± 0.1	0.05 ± 00.1**
GAL-Ag@AuNPs	1.49 ± 0.15*	0.77 ± 0.02*	0.032 ± 0.001**	0.74 ± 0.1	0.74 ± 0.04**
GAL	1.67 ± 0.3*	1.23 ± 0.43**	0.057 ± 0.004*	0.55 ± 0.21	0.55 ± 0.03*
TAN-Ag@AuNPs	0.43 ± 0.088	0.35 ± 0.092	0.32 ± 0.09	0.66 ± 0.11	0.39 ± 0.01
TAN	0.49 ± 0.08	0.29 ± 0.035	0.3 ± 0.06	0.57 ± 0.09	0.45 ± 0.012
ECG-Ag@AuNPs	1.5 ± 0.3*	0.79 ± 0.029*	0.017 ± 0.001**	0.85 ± 0.06	0.97 ± 0.11*
EGG	1.7 ± 0.45**	0.88 ± 0.124*	0.018 ± 0.001**	1.05 ± 0.13**	1.05 ± 0.11*
PRO-Ag@AuNPs	1.27 ± 0.3*	0.75 ± 0.1*	0.14 ± 0.09*	0.75 ± 0.07	0.75 ± 0.089*
PRO	1.62 ± 0.4**	0.7 ± 0.02*	0.09 ± 0.001**	0.62 ± 0.15	0.62 ± 0.1*
RES-Ag@AuNPs	1.1 ± 0.1*	0.9 ± 0.092*	0.11 ± 0.09*	0.52 ± 0.095	0.52 ± 0.1*
RES	1.3 ± 0.093*	1 ± 0.126**	0.13 ± 0.02*	0.36 ± 0.1	0.36 ± 0.08

Note: *Represents significant differences with $p \leq 0.05$, while **means $p \leq 0.01$.
Abbreviations: TAN, tannic acid modified; GAL, gallic acid modified; ECG, epicatechin gallate modified; RES, resveratrol modified and PRO, procyanidin modified; PCNA, proliferating cell nuclear antigen; MMP-9, matrix metalloproteinase 9; S.E.M., standard error of mean.

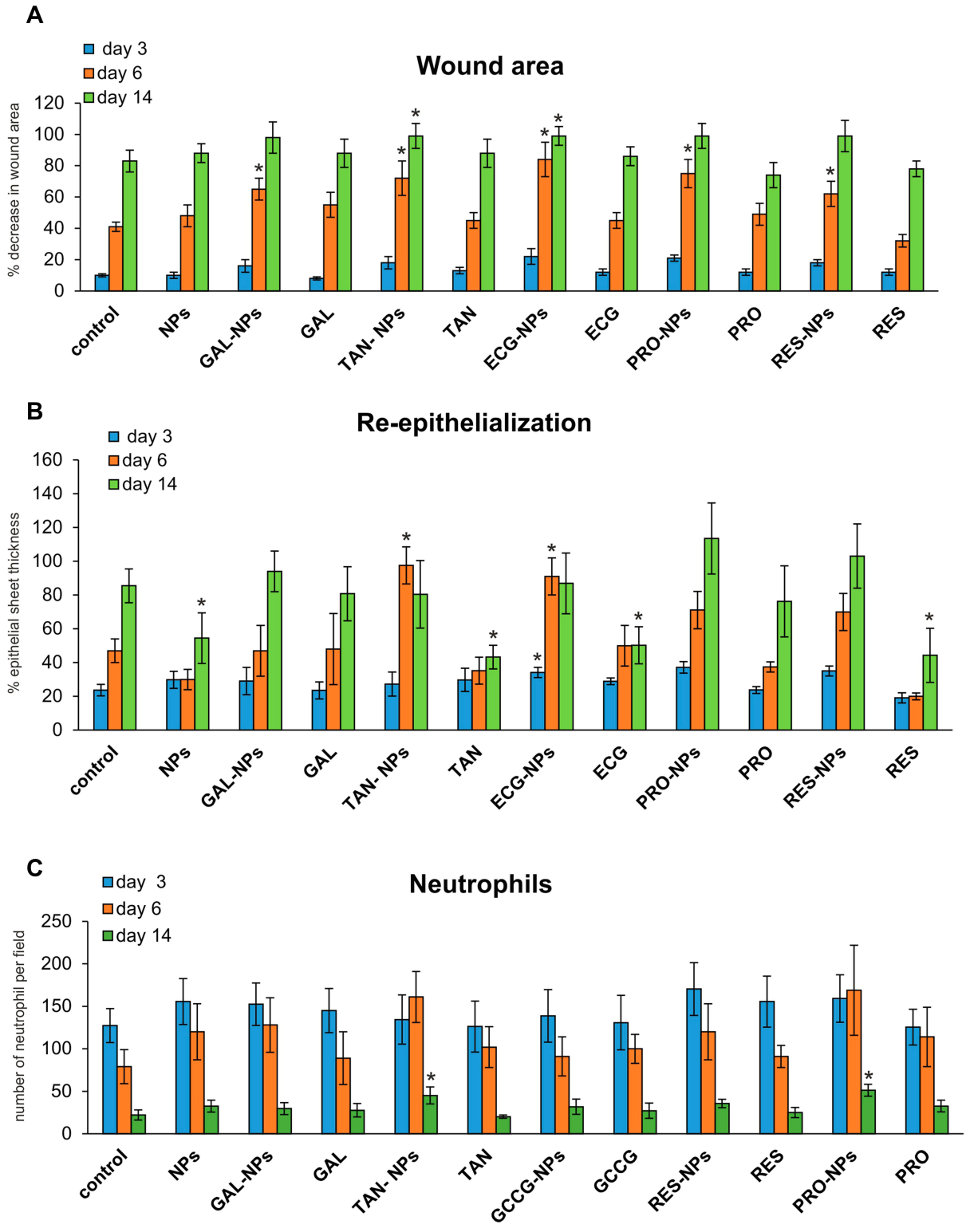

Figure 6 Au@AgNPs modified with selected polyphenols (tannic acid, gallic acid, resveratrol, epicatechin gallate and procyanidin B2) improve healing in a mouse wound model. Modified and unmodified Au@AgNPs as well as solutions of polyphenols used for modification were applied at 5 μg/mL in saline and the wounds were subjected to further tests at 3, 6 and 14 days from injury. Each bar represents the mean from 5 animals ± S.E.M (N=5). (**A**) Percentage of the original wound size at day 6 from wounding. (**B**) Re-epithelialization, expressed as the epithelial sheet thickness in μm measured in hematoxylin-eosin stained tissue sections at respective days after injury. (**C**) Numbers of neutrophils per field in the skin sections subjected to hematoxylin-eosin staining at respective days after injury (magnification 400 x). *p ≤ 0.05 versus untreated control.
Abbreviations: NPs, Au@AgNPs; ECG, epicatechin gallate modified; GAL, gallic acid modified; PRO, procyanidin B2 modified; RES, resveratrol modified; TAN, tannic acid modified; S.E.M., standard error of mean.

in comparison to control group, and it continued at day 14, also for and PRO-Au@AgNPs ($p \leq 0.05$) (Figure 6C, Supplementary Figure 2).

Polyphenol-Modified Ag/AuNPs Do Not Induce Toxic Dermal Reaction

The basic principle underlying the murine local lymph node assay (LLNA) is that sensitizers induce proliferation of lymphocytes in the lymph nodes draining the site of substance application (auricle). This proliferation is proportional to the dose applied, and provides means of obtaining an objective, quantitative measurement of sensitization. Here, we used a nonradiolabelled 5-bromo-2-deoxyuridine (BrdU) with detection by an enzyme-linked immunosorbent assay (ELISA) to assess lymphocyte proliferation. In lymph nodes isolated from ears treated with a sensitizer – citral, we found a significant proliferative response ($p = 0.009$), while lymphocyte proliferation in Au@AgNPs, RES- and ECG-Au@AgNPs-treated animals was at the level similar to control mice (Figure 8). Interestingly, corresponding polyphenol – resveratrol (RES) and epicatechin gallate (ECG) caused significant down-regulation of lymphocyte proliferation ($p \leq 0.01$) (Figure 8). Similarly, other polyphenol conjugates as well as corresponding polyphenol solutions, such as GAL-, TAN- and PRO-Au@AgNPs caused a significant decrease of lymphocyte proliferation ($p \leq 0.05$) (Figure 8).

Polyphenol-Modified Ag/AuNPs Differently Modulate Expression of Cytokines in Wounds

The mRNA levels of tumour necrosis factor-α (TNF-α), transforming growth factor β1 (TGF-β1), interleukin 1β (IL-1β), vascular endothelial growth factor-α (VEGF-α) and platelet-derived growth factor-β (PDGF-β) were measured by qRT-PCR (Figure 9). In general, mRNA expressions of detected cytokines were increased in all treated groups at day 3 of wound repair in comparison to control wounds (Figure 9). However, the levels of mRNAs upregulation differed between the treatment groups. At day 3, wounds treated with ECG- or RES-Au@AgNPs and the corresponding polyphenol solutions showed the highest up-regulation of mRNA for TNF-α (Figure 9), while only Au@AgNPs and their modifications with RES and ECG caused significant up-regulation of TGF-β1 mRNA ($p \leq 0.05$) (Figure 9). Similarly, polyphenol modifications of Au@AgNPs showed higher up-regulation of PDGF-β mRNA levels in comparison to corresponding polyphenol solutions ($p \leq 0.05$) (Figure 9), except for procyanidin B2 modification. For IL-1β mRNA, the highest levels were detected at day 3 for ECG- or RES-Au@AgNPs. The levels of mRNA for TNF-α, IL-1β, TGF-β1 and PDGF-β decreased until day 6, except for unmodified Au@AgNPs, showing high levels of TNF-α mRNA at day 14 (Figure 9). The levels of mRNA for VEGF-α were significantly up-regulated at day 14 for the wounds treated with unmodified Au@AgNPs and modified with resveratrol and epicatechin gallate ($p \leq 0.05$) (Figure 9).

Discussion

Polyphenols have been widely used in traditional medicine to treat several chronic skin diseases, such as psoriasis and vitiligo, and they are also known to be therapeutically beneficial in wound healing and show anti-inflammatory effects when applied topically.[29,30] Each bioactive agent may have specific function on wound healing properties, influencing different stages of this process. Wound dressings containing AgNPs can effectively protect an injury from bacterial infection and promote tissue regeneration during the healing process.[31,32] Previously, we showed that AgNPs sized >26 nm modified with 340 μM tannic acid (TA-AgNPs) promoted wound healing both in vivo and in vitro by accelerating re-epithelialization.[16] We reported that TA-AgNPs sized >26 nm induced little cytotoxicity in both mouse and human keratinocytes as well as fibroblasts in vitro. However, an increased toxicity was found in mouse monocytes, showing intensive internalization of TA-AgNPs.[15,33] The internalisation-related toxicity was size-dependent, with 13 nm TA-AgNPs being the strongest inducers of ROS production.[15,33]

In this study, we used bimetallic Au@AgNPs, sized 30 nm, to reduce previously observed cytotoxicity and to test if we can combine wound healing properties of nanoparticles with particular properties of different polyphenols (Supplementary Figure 1). First, we chose polyphenols from the green tea extracts, known to influence skin healing on the basis of the literature review. Next, we prepared conjugates of selected polyphenols with 30 nm Au@AgNPs and used for toxicity screening. Out of approx. 100 polyphenols used to modify Au@AgNPs, only several showed little, or no toxicity, depending on the concentration used for modification. These polyphenols included: tannic acid, gallic acid, polydatin, resveratrol, catechin, epicatechin, epigallocatechin, epicatechin gallate, epigallocatechin gallate and procyanidin B2 at different concentrations (Table 1). The toxicity of both Au@AgNPs and polyphenol-modified Au@AgNPs was

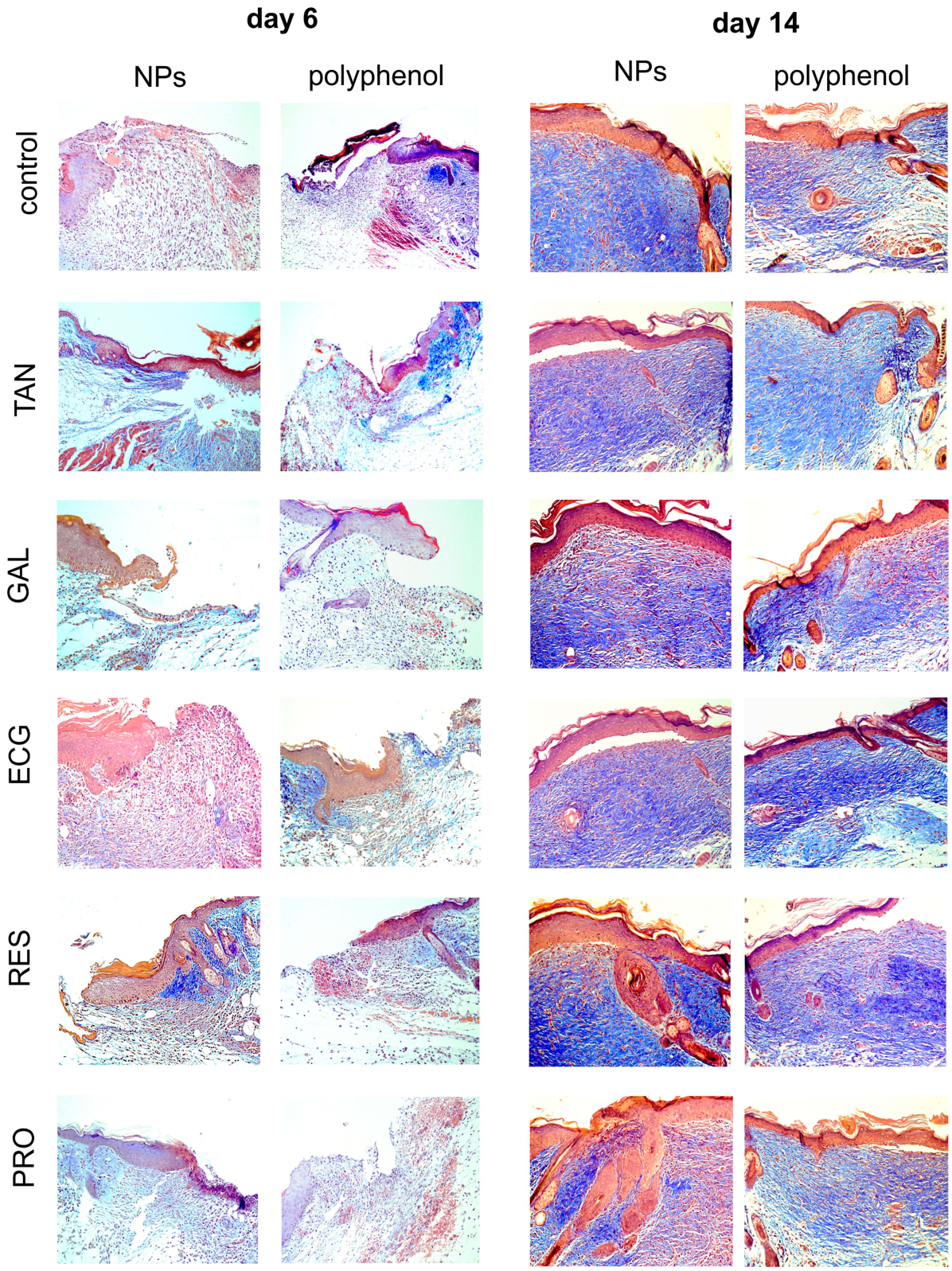

Figure 7 General morphology of wounds after treatment with unmodified and polyphenol-modified Au@AgNPs. Representative microphotographs of the Tri-chrome Masson stained wound sections at 6 and 14 day post-injury. Modified and unmodified Au@AgNPs as well as solutions of polyphenols used for modification were applied at 5 μg/mL in saline. Magnification x 400.

Abbreviations: NPs, Au@AgNPs; ECG, epicatechin gallate modified; GAL, gallic acid modified; PRO, procyanidin B2 modified; RES, resveratrol modified; TAN, tannic acid modified.

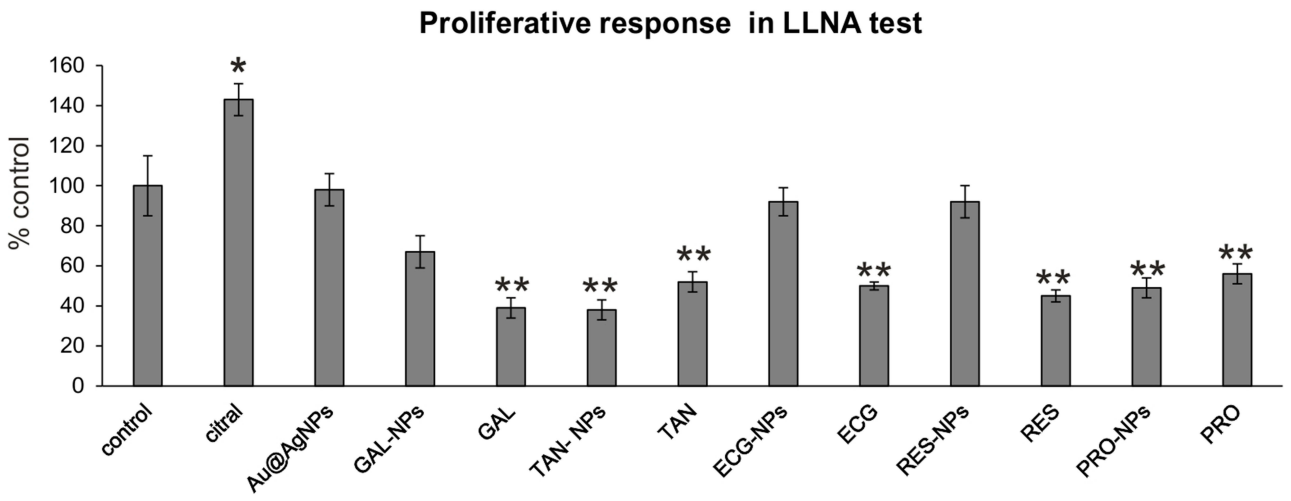

Figure 8 Polyphenol-modified Au@AgNPs do not induce toxic dermal reaction. The murine local lymph node assay (LLNA) was used to test inflammatory ear reaction upon Ag/AuNPs exposure. Mice were subjected to ear stripping followed by three applications of unmodified and tannin-modified Au@AgNPs (25 µg per each ear, every 24 h). Citral was used as a positive control. Proliferative response of lymphocytes isolated from auricle lymph nodes was measured by BrdU test at 72 h after stimulation with concanavalin A. Each bar represents the mean from 3 animals ± S.E.M (N=3), *means significant differences with $p \leq 0.05$, while **means $p \leq 0.001$ in comparison to negative control (vehicle).

Abbreviations: NPs, Au@AgNPs; ECG, epicatechin gallate modified; GAL, gallic acid modified; PRO, procyanidin B2 modified; RES, resveratrol modified; TAN, tannic acid modified; S.E.M., standard error of mean.

very low, except for the highest concentrations of modification with tannic acid (340 µM) and epigallocatechin gallate (200 µM) (Table 1). This toxicity was related to ROS production (Table 2). Furthermore, polyphenol-conjugated Au@AgNPs showed little internalization by HaCaT cells, which was related to low toxicity (Figure 4). Low toxicity of bimetallic Au@AgNPs was also shown by other authors for HaCat cells, red blood cells[34] and HEK293 cells.[35]

In order to select the most promising conjugates for further studies, we used in vitro scratch assay to screen for the ability to stimulate keratinocyte migration (Figure 3). We found that migration of keratinocytes into the wounded area was dependent on the type of the polyphenol used to modify Au@AgNPs, but also on its concentration. Our goal was to select modifications of Au@AgNPs, showing the highest additive effect for wound healing in comparison to polyphenol solution itself. Only five combinations fulfilled this requirement: 15 µM tannic acid, 200 µM resveratrol, 200 µM epicatechin gallate, 1000 µM gallic acid and 200 µM procyanidin B2 (Figure 3) and were used for further in vitro and in vivo studies.

Epithelial-to-mesenchymal transition (EMT) is a tightly regulated physiological process in which epithelial cells undergo multiple morphologic, biochemical and genetic changes enabling them to acquire a mesenchymal phenotype.[36,37] The process of re-epithelialization is sometimes termed as "partial EMT".[38] A hallmark of EMT is cell-cell dissociation and acquisition of motility. During re-epithelialization keratinocytes at the wound edge lose their intercellular adhesions and migrate across the wound.[38] EMT is also characterised by the loss of epithelial cell markers, such as E-cadherin.[36,37] The cell then progresses towards a mesenchymal phenotype, accompanied by a temporally regulated expression of proteins including neural cadherin (N-cadherin), vimentin, integrin, fibronectin, and matrix metalloproteinases (MMPs).[36–39] Pathological EMT is present in many inflammatory diseases and leads to tissue fibrosis, loss of organ function, cancer progression and metastasis.[36,37] Gliga et al, used a model of non-tumorigenic, SV40 transformed human lung BEAS-2B cells to show that repeated low-dose, long-term exposure of these cells to AgNPs sized 10 and 75 nm is pro-fibrotic, induces EMT and cell transformation.[40] On the other hand, many polyphenols have been shown to regulate excessive EMT, such as tannic acid, gallic acid, epicatechin gallate, procyanidin B2 and resveratrol.[41]

Here, we found that polyphenols and polyphenol-modified Au@AgNPs induced proliferation of HaCaT cells, except for unmodified Au@AgNPs and TA-AuAgNPs (Figure 5). Interestingly, while other conjugates up-regulated expression of E-cadherin (Figure 5, Table 3), they also down-regulated production of a soluble

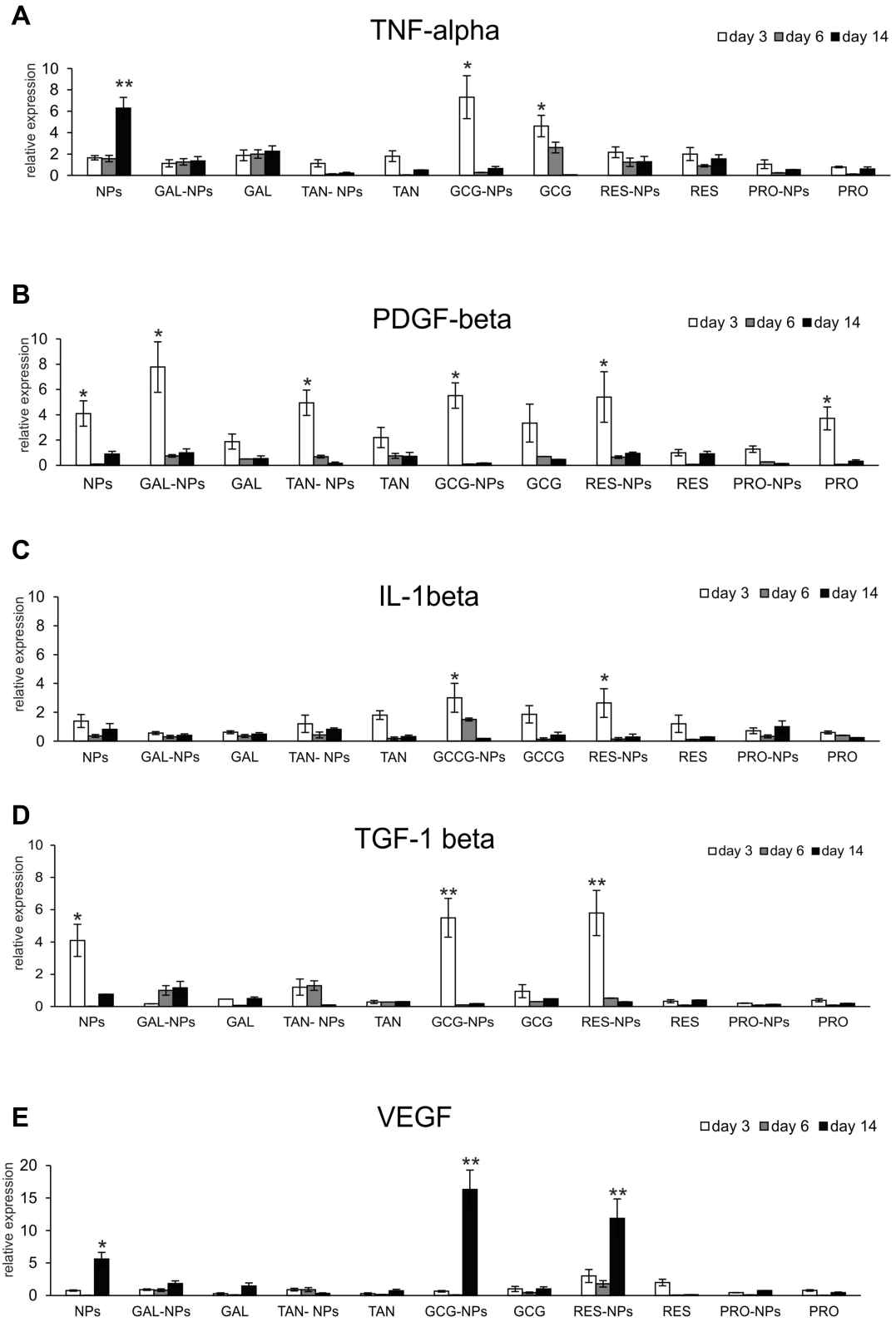

Figure 9 Cytokine expression changes in wounds subjected to treatment with unmodified and polyphenol-modified Au@AgNPs at 3, 6 and Comment: Dear author, please advise should 7 day be changed to 14 day instead as per figure images. 14 day from injury. mRNA levels of TNF-α (**A**), PDGF-β (**B**), IL-1β (**C**), TGF-β1 (**D**) and VEGF (**E**) were expressed as expression relative to control on the basis of the 2ΔCt method. mRNA levels were counted from three PCR reactions for each sample. N=3. *Means significant differences with $p \leq 0.05$, while **means $p \leq 0.001$ in comparison to control.

Abbreviations: NPs, Au@AgNPs; TAN, tannic acid modified; GAL, gallic acid modified; ECG, epicatechin gallate modified; RES, resveratrol modified; PRO, procyanidin B2 modified.

E-cadherin form (80 kDa). Up-regulation of E-cadherin by certain polyphenols has been shown before.[41] Epicatechin gallate and resveratrol can reverse TGF-β1-induced epithelial-to-mesenchymal transition by up-regulation of E-cadherin and involucrin.[42,43] Metalloproteinases (MMPs) are zinc-dependent endopeptidases and key molecules in the healing process and tissue remodelling. They are capable of degrading all kinds of extracellular matrix proteins, thus helping in cell migration and wound closure. However, increased levels of MMPs are also found in chronic wounds, such as diabetic ulcers, characterised with excessive inflammation.[44] AgNPs have been shown to have no influence upon MMP-2 and MMP-9 secretion[45,46] and we also found that unmodified Au@AgNPs as well as TAN-Au@AgNPs did not influence MMP-9 expression (Figure 5). Other tested polyphenol conjugates induced expression of MMP-9 (Figure 5).

Taken together, we can conclude that wound healing by TAN-Au@AgNPs is mediated through a presumably different process than this induced by other tested polyphenols (RES-, GAL-, ECG- and PRO-Au@AgNPs). TAN-Au @AgNPs induce more EMT-like re-epithelialization than other polyphenol modifications of Au@AgNPs, acting through proliferation and wound closure rather than migration of keratinocytes. Previous studies showed that TAN might directly interact with TGF-β1, thereby repressing TGF-β signalling and subsequent EMT process in epithelial cells.[47] However, it is also possible that upon conjugation with NPs, especially in low doses, this activity of TAN is diminished.

Previously, we showed that treatment of the same in vivo model with 33 and 46 nm TAN-AgNPs led to a faster wound closure and increased re-epithelialization compared with control mice.[16] Similarly as here, we did not observe better wound healing with uncoated AgNPs. However, other authors showed that uncoated AgNPs sized 5–15 nm but also those with a diameter of ~20 nm accelerated re-epithelialization, enhanced migration of fibroblasts and reduced neutrophil and macrophage infiltration at the wound site in rodent models.[48,49] In this study, we found that modification of bimetallic nanoparticles with selected polyphenols leads to the improvement of wound healing, although particular polyphenols may show different effects upon its subsequent stages. Additionally, application of polyphenol-modified Au@AgNPs onto the stratified ear skin in LLNA test did not lead to the local irritation or inflammation. Furthermore, some modifications also showed anti-inflammatory potentials, such as GAL-, TAN- and PRO-Au@AgNPs (Figure 8).

Tannic acid (TAN) is a plant polyphenol found abundantly in the galls of *Quercus* species, and it is categorized as an antioxidant, antimicrobial, antiviral, and anti-inflammatory agent.[50,51] Structurally, TAN has a glucose moiety as a core, and the hydroxyl groups of glucose are esterified with five digallic acids.[50,51] Chen et al, demonstrated that TAN can accelerate wound healing through modulation of inflammatory cytokines and growth factors as well as through activation of ERK1/2 pathway.[52] We also found that TAN-modified but not unmodified AgNPs down-regulated inflammatory response in HaCaT keratinocytes subjected to TNF-α and LPS, as well as induced ERK 1/2 pathway.[15] We previously used AgNPs modified with 340 μM TAN, while here we managed to obtain a similar healing effect with a decreased concentration of tannic acid, and without toxicity. Previously, we also showed that expression of VEGF-α, TGF-1β and PDGF was induced by both tannic acid modified and unmodified AgNPs early during wound healing. However, this effect could be contributed to the AgNPs rather than tannic acid modification.[16] Au@AuNPs modified with 15 μM tannic acid showed up-regulation of only PDGF-α only early during proliferative phase and again, this should be contributed to the activity of nanoparticles (Figure 9).

As mentioned, TAN is a polymer of gallic acid (GA).[50,51] Gallic acid is a 3,4,5-trihydoxybenzoic acid, a phenolic acid found in almost all plants including fruits, leaves, and wild flowers.[53] It has been reported to possess antioxidant, anti-inflammatory, analgesic, and anticancer properties.[53–55] Kapoor et al, showed that GA induced cell cycle arrest at G1 phase and promoted apoptosis in fibroblasts derived from keloids.[56] GA inhibited AKT and ERK1/2 activity in fibroblasts in a dose-dependent manner.[56] Here we found that GA did not show any inhibitory effects upon keratinocyte proliferation, which is consistent with other studies by Yang et al demonstrating that GA is beneficial to wound healing by promoting the migration of keratinocytes and fibroblasts under normal and hyperglucidic conditions.[57] However, GAL-Au @AgNPs showed no significant up-regulation of cytokines related to wound healing, except for PDGF-α (Figure 9).

Catechins are naturally occurring polyphenolic compounds with putative anti-inflammatory, antioxidant and free radical scavenging effects in vitro.[58–60] By using a full-thickness incisional model of wound healing in rats Kapoor et al showed a significant improvement in the quality of scar formation and an increase in the number of new blood vessels in the ECG-treated group, correlating

with high levels of VEGF.[56] In our study, ECG-modified Au@AgNPs showed the highest wound healing potential. ECG-Au@AgNPs also induced expression of TNF-α, IL-1β and PDGF early during wound healing (inflammation phase) and this effect could be contributed to ECG itself rather than NPs. TGF-1β and VEGF levels were increased by ECG-Au@AgNPs during inflammation and proliferative phases of healing, respectively (Figure 9). TGF-β1 plays an important role in almost all stages of wound healing and scar formation and AgNPs can upregulate TGF-β1 early during wound healing process.[61] Gurunathan et al have demonstrated that AgNPs inhibited VEGF-induced cell proliferation, migration, and capillary-like tube formation of bovine retinal endothelial cells as well as effectively inhibited the formation of new blood microvessels induced by VEGF.[62] Both here and previously,[16] we observed an opposite effect, with ECG-Au@AgNPs inducing VEGF upregulation during wound healing. However, this effect seems to be specifically related to the silver nanoparticle core/shell rather than a specific polyphenol modification.

Resveratrol (RES) consists 3,5,40-trihydroxytrans-stilbene, and it is one of the best-studied phytophenols with pleiotropic properties.[63,64] Resveratrol inhibits VEGF-induced angiogenesis in endothelial cells[65] and inhibits TNF-α-induced keratinocyte proliferation and matrix metalloproteinase (MMP-9) expression by inhibiting nuclear factor (NF)-kappa B and activator protein-1 (AP-1).[65] RES also suppresses type I collagen deposition and keloid fibroblast proliferation.[66] In this study, RES did not influence keratinocyte proliferation but it inhibited MMP-9 and TNF-α expression (Figure 5, Table 3). RES can inhibit EMT in colorectal cancer through the TGF-β1/Smads signaling pathway[67] as well as PDGF-β-induced migration of retinal pigment epithelial cells.[68] Here, RES-Au@AgNPs induced expression of TGF-β1 and PDGF-β expression during inflammatory phase of wound healing (Figure 9). Furthermore, RES-Au@AgNPs also induced expression of VEGF in the remodelling phase (Figure 9). This implies that the presence of silver in this particular conjugate modifies polyphenol properties related to EMT and angiogenesis. Still, RES-Au@AgNPs showed anti-inflammatory properties, as found in LLNA test.

Proanthocyanidins are a species of phenolic compounds that take the form of polymers or oligomers built of flavan-3-ol units, such as catechin, epicatechin, gallocatechin, epigallocatechin, afzelechin, and epiafzelechin.[69] The most ubiquitous proanthocyanidin present in natural source is the procyanidin B2, where the flavan-3-ols are linked via an interflavan bond between the benzylic C-4 carbon of the heterocyclic ring of the upper unit and the C-8 carbon of the flavan-3-ol A-ring of the lower unit (4→8).[70] Procyanidin B2 possesses anti-microbial and antioxidant properties and it induces anti-inflammatory M2 polarization of macrophages.[71] Takahashi et al found that procyanidin oligomers promote the proliferation of mouse hair epithelial cells.[72] Here, procyanidin B2 promoted wound healing both in vitro and in vivo, and showed anti-inflammatory activity (Figures 3, 6–8). Surprisingly, PRO-Au@AgNPs up-regulated neutrophil accumulation late during wound healing (14 d) despite no up-regulation of pro-inflammatory cytokines.

Conclusion

The results of this study have demonstrated, for the first time, that treatment with bimetallic Au@AgNPs modified with selected polyphenols results in a significant improvement of wound healing both in vitro and in vivo. In addition, we have demonstrated that particular polyphenols used to modify bimetallic nanoparticles may show different effects upon different stages of wound healing. Taking into account the ability of bimetallic nanoparticles to penetrate injured skin and interact with the skin immune system, we can assume that combining Au@AgNPs with selected polyphenols allows to prepare a new type of nanomaterials, precisely tailored for the requirements of different types of injuries, such as chronic, infected or hyperproliferative wounds.

Acknowledgments

This work was supported by the National Science Centre Poland grant no. 2014/13/B/NZ5/01356.

Author Contributions

All authors made substantial contributions to conception and design, acquisition of data, or analysis and interpretation of data; took part in drafting the article or revising it critically for important intellectual content; gave final approval of the version to be published; and agree to be accountable for all aspects of the work.

Disclosure

The authors report no conflicts of interest in this work.

References

1. Balasundrama N, Sundramb K, Sammana S. Phenolic compounds in plants and agri-industrial by-products: antioxidant activity, occurrence, and potential uses. *Food Chem*. 2006;99:191–203. doi:10.1016/j.foodchem.2005.07.042
2. Okuda T. Systematics and health effects of chemically distinct tannins in medicinal plants. *Phytochemistry*. 2005;66:2012–2031. doi:10.1016/j.phytochem.2005.04.023
3. Serrano J, Puupponen-Pimia R, Dauer A, Aura AM, Saura-Calixto F. Tannins: current knowledge of food sources, intake, bioavailability and biological effects. *Mol Nutr Food Res*. 2009;53(Suppl 2):S310–S329. doi:10.1002/mnfr.200900039
4. Arct J, Pytkowska K. Flavonoids as components of biologically active cosmeceuticals. *Clin Dermatol*. 2008;26:347–357. doi:10.1016/j.clindermatol.2008.01.004
5. Carrera-Quintanar L, López Roa RI, Quintero-Fabián S, Sánchez-Sánchez MA, Vizmanos B, Ortuño-Sahagún D. Phytochemicals that influence gut microbiota as prophylactics and for the treatment of obesity and inflammatory diseases. *Mediators Inflamm*. 2018;26:9734845.
6. Alkhalidy H, Wang Y, Liu D. Dietary flavonoids in the prevention of T2D: an overview. *Nutrients*. 2018;10(4):pii: E438. doi:10.3390/nu10040438
7. Wu JM, Wang ZR, Hsieh TC, Bruder JL, Zou JG, Huang YZ. Mechanism of cardioprotection by resveratrol, a phenolic antioxidant present in red wine (Review). *Int J Mol Med*. 2001;8:3–17. doi:10.3892/ijmm.8.1.3
8. Ma T, Tan MS, Yu JT, Tan L. Resveratrol as a therapeutic agent for Alzheimer's disease. *Biomed Res Int*. 2014;2014:350516. doi:10.1155/2014/350516
9. Cipolletti M, Solar Fernandez V, Montalesi E, Marino M, Fiocchetti M. Beyond the antioxidant activity of dietary polyphenols in cancer: the modulation of estrogen receptors (ERs) signaling. *Int J Mol Sci*. 2018;19(9):pii: E2624. doi:10.3390/ijms19092624
10. Mahata D, Nag A, Nando GB, Mandal SM, Franco OL. Self-assembled tea tannin graft copolymer as nanocarriers for antimicrobial drug delivery and wound healing activity. *J Nanosci Nanotechnol*. 2018;18:2361–2369. doi:10.1166/jnn.2018.14307
11. Bueno FG, Panizzon GP, Mello EV, et al. Hydrolyzable tannins from hydroalcoholic extract from Poincianella pluviosa stem bark and its wound-healing properties: phytochemical investigations and influence on in vitro cell physiology of human keratinocytes and dermal fibroblasts. *Fitoterapia*. 2014;99:252–260. doi:10.1016/j.fitote.2014.10.007
12. Schreml S, Szeimies RM, Prantl L, Landthaler M, Babilas P. Wound healing in the 21st century. *J Am Acad Dermatol*. 2010;63:866–881. doi:10.1016/j.jaad.2009.10.048
13. Martin P, Nunan R. Cellular and molecular mechanisms of repair in acute and chronic wound healing. *Br J Dermatol*. 2015;173:370–378. doi:10.1111/bjd.13954
14. Kalan LR, Brennan MB. The role of the microbiome in nonhealing diabetic wounds. *Ann N Y Acad Sci*. 2019;1435:79–92. doi:10.1111/nyas.13926
15. Orlowski P, Soliwoda K, Tomaszewska E, et al. Toxicity of tannic acid-modified silver nanoparticles in keratinocytes: potential for immunomodulatory applications. *Toxicol in Vitro*. 2016;35:43–54. doi:10.1016/j.tiv.2016.05.009
16. Orlowski P, Zmigrodzka M, Tomaszewska E, et al. Tannic acid-modified silver nanoparticles for wound healing: the importance of size. *Int J Nanomedicine*. 2018;16:991–1007. doi:10.2147/IJN.S154797
17. Loo YY, Rukayadi Y, Nor-Khaizura MA, et al. *In vitro* antimicrobial activity of green synthesized silver nanoparticles against selected Gram-negative foodborne pathogens. *Front Microbiol*. 2018;16(9):1555. doi:10.3389/fmicb.2018.01555
18. Mott DM, Anh DT, Singh P, Shankar C, Maenosono S. Electronic transfer as a route to increase the chemical stability in gold and silver core–shell nanoparticles. *Adv Colloid Interface Sci*. 2012;185–-186:14–33. doi:10.1016/j.cis.2012.08.007
19. Morriss RH, Collins LF. Optical properties of multilayer colloids. *J Chem Phys*. 1964;41:3357–3363. doi:10.1063/1.1725733
20. Banerjee M, Sharma S, Chattopadhyay A, Ghosh SS. Enhanced antibacterial activity of bimetallic gold-silver core–shell nanoparticles at low silver concentration. *Nanoscale*. 2011;3:5120–5125. doi:10.1039/c1nr10703h
21. Hamidi-Asl E, Dardenne F, Pilehvar S, Blust R, De Wael K. Unique properties of core shell Ag@Au nanoparticles for the aptasensing of bacterial cells. *Chemosensors*. 2016;4:16. doi:10.3390/chemosensors4030016
22. Perez-Lloret M, Fraix A, Petralia S, et al. One-step photochemical green synthesis of water-dispersible Ag, Au, and Au@Ag core–shell nanoparticles. *Chemistry*. 2019;25:14638–14643. doi:10.1002/chem.201903076
23. Loiseau A, Zhang L, Hu D, et al. Core−shell gold/silver nanoparticles for localized surface plasmon resonance-based naked-eye toxin biosensing. *ACS Appl Mater Interfaces*. 2019;11:46462–46471. doi:10.1021/acsami.9b14980
24. Lu L, Wang H, Zhou Y, et al. Seed-mediated growth of large, monodisperse core-shell gold-silver nanoparticles with Ag-like optical properties. *Chem Commun*. 2002;21:144–145.
25. Rhodes LE, Darby G, Massey K, et al. Oral green tea catechin metabolites are incorporated into human skin and protect against UV radiation-induced cutaneous inflammation in association with reduced production of pro-inflammatory eicosanoid 12-hydroxyeicosatetraenoic acid. *Br J Nutr*. 2013;110(5):891–900. doi:10.1017/S0007114512006071
26. Berman A, Motechin R, Wiesenfeld M, Holz M. The therapeutic potential of resveratrol: a review of clinical trials. *Precis Oncol*. 2019;1:35. doi:10.1038/s41698-017-0038-6
27. Soliwoda K, Tomaszewska E, Tkacz-Szczesna B, et al. The influence of the chain length and the functional group steric accessibility of thiols on the phase transfer efficiency of gold nanoparticles from water to toluene. *Polish J Chem Technol*. 2014;16:86–91. doi:10.2478/pjct-2014-0015
28. Liang CC, Park AY, Guan JL. In vitro scratch assay: a convenient and inexpensive method for analysis of cell migration in vitro. *Nat Protoc*. 2007;2:329–333. doi:10.1038/nprot.2007.30
29. Korkina L, De Luca C, Pastore S. Plant polyphenols and human skin: friends or foes. *Ann N Y Acad Sci*. 2012;1259(1):77–86. doi:10.1111/j.1749-6632.2012.06510.x
30. Tuong W, Walker K, Sivamani RK. Polyphenols as novel treatment options for dermatological diseases: a systematic review of clinical trials. *J Dermatolog Treat*. 2015;26:381–388. doi:10.3109/09546634.2014.991675
31. Morones JR, Elechiguerra JL, Camacho A, et al. The bactericidal effect of silver nanoparticles. *Nanotechnology*. 2005;16:2346–2353. doi:10.1088/0957-4484/16/10/059
32. Tian J, Wong KK, Ho CM, et al. Topical delivery of silver nanoparticles promotes wound healing. *Chem Med Chem*. 2007;2:129–136. doi:10.1002/cmdc.200600171
33. Orlowski P, Krzyzowska M, Zdanowski R, et al. Assessment of in vitro cellular responses of monocytes and keratinocytes to tannic acid modified silver nanoparticles. *Toxicol in Vitro*. 2013;27:1798–1808. doi:10.1016/j.tiv.2013.05.010
34. Kumar S, Majhi RK, Singh A, et al. Carbohydrate-coated gold–silver nanoparticles for efficient elimination of multidrug resistant bacteria and *in vivo* wound healing. *ACS App Mater Interfaces*. 2019;11:42998–43017. doi:10.1021/acsami.9b17086
35. Katifelis H, Lyberopoulou A, Mukha I, et al. Ag/Au bimetallic nanoparticles induce apoptosis in human cancer cell lines via P53, CASPASE-3 and BAX/BCL-2 pathway. *Artif Cells Nanomed Biotechnol*. 2018;46(sup3):S389–S398. doi:10.1080/21691401.2018.1495645

36. Thiery JP, Acloque H, Huang RY, Nieto MA. Epithelial-mesenchymal transitions in development and disease. *Cell*. 2009;139:871–890. doi:10.1016/j.cell.2009.11.007
37. Savagner P. The epithelial-mesenchymal transition (EMT) phenomenon. *Ann Oncol*. 2010;21(Suppl7):vii89–vii92. doi:10.1093/annonc/mdq292
38. Arnoux V, Come C, Kusewitt D, Hudson L, Savagner P. Cutaneous wound reepithelialization: a partial and reversible EMT. In: Savagner P, editor. *Rise and Fall of Epithelial Phenotype: Concepts of Epithelial-Mesenchymal Transition*. Berlin: Springer; 2005:111–134.
39. Huang RY, Guilford P, Thiery JP. Early events in cell adhesion and polarity during epithelial-mesenchymal transition. *J Cell Sci*. 2012;125:4417–4422. doi:10.1242/jcs.099697
40. Gliga AR, Di Bucchianico S, Lindvall J, Fadeel B, Karlsson HL. RNA-sequencing reveals long-term effects of silver nanoparticles on human lung cells. *Sci Rep*. 2018;8(1):6668. doi:10.1038/s41598-018-25085-5
41. Avila-Carrasco L, Majano P, Sánchez-Toméro JA, et al. Natural plants compounds as modulators of epithelial-to-mesenchymal transition. *Front Pharmacol*. 2019;10:715. doi:10.3389/fphar.2019.00715
42. Huang SF, Horng CT, Hsieh YS, Hsieh YH, Chu SC, Chen PN. Epicatechin-3-gallate reverses TGF-β1-induced epithelial-to-mesenchymal transition and inhibits cell invasion and protease activities in human lung cancer cells. *Food Chem Toxicol*. 2016;94:1–10. doi:10.1016/j.fct.2016.05.009
43. Wang H, Zhang H, Tang L, et al. Resveratrol inhibits TGF-β1-induced epithelial-to-mesenchymal transition and suppresses lung cancer invasion and metastasis. *Toxicology*. 2013;303:139–146. doi:10.1016/j.tox.2012.09.017
44. Verma RP, Hansch C. Matrix metalloproteinases (MMPs): chemical-biological functions and (Q)SARs. *Bioorg Med Chem*. 2007;15:2223–2268. doi:10.1016/j.bmc.2007.01.011
45. Vila L, Marcos R, Hernández A. Long-term effects of silver nanoparticles in caco-2 cells. *Nanotoxicology*. 2017;11:771–780. doi:10.1080/17435390.2017.1355997
46. Franková J, Pivodová V, Vágnerová H, Juráňová J, Ulrichová J. Effects of silver nanoparticles on primary cell cultures of fibroblasts and keratinocytes in a wound-healing model. *J Appl Biomater Funct Mater*. 2016;14(2):e137–e142. doi:10.5301/jabfm.5000268
47. Pattarayan D, Sivanantham A, Krishnaswami V, et al. Tannic acid attenuates TGF-β1-induced epithelial-to-mesenchymal transition by effectively intervening TGF-β signaling in lung epithelial cells. *J Cell Physiol*. 2018;233:2513–2525. doi:10.1002/jcp.26127
48. Kwan KH, Liu X, To MK, Yeung KW, Ho CM, Wong KK. Modulation of collagen alignment by silver nanoparticles results in better mechanical properties in wound healing. *Nanomedicine*. 2011;7:497–504. doi:10.1016/j.nano.2011.01.003
49. Neibert K, Gopishetty V, Grigoryev A, et al. Wound-healing with mechanically robust and biodegradable hydrogel fibers loaded with silver nanoparticles. *Adv Healthc Mater*. 2012;1:621–630. doi:10.1002/adhm.201200075
50. Fernandez O, Capdevila JZ, Dalla G, Melchor G. Efficacy of Rhizophora mangle aqueous bark extract in the healing of open surgical wounds. *Fitoterapia*. 2002;73:564–568. doi:10.1016/S0367-326X(02)00229-0
51. Buzzini P, Arapitsas P, Goretti M, et al. Antimicrobial and antiviral activity of hydrolysable tannins. *Mini-Rev Med Chem*. 2008;8:1179–1187. doi:10.2174/138955708786140990
52. Chen Y, Tian L, Yang F, et al. Tannic acid accelerates cutaneous wound healing in rats via activation of the ERK 1/2 signaling pathways. *Adv Wound Care*. 2019;8:341–354. doi:10.1089/wound.2018.0853
53. Ng TB, He JS, Niu SM, et al. A gallic acid derivative and polysaccharides with antioxidative activity from rose (Rosa rugosa) flowers. *J Pharm Pharmacol*. 2004;56:537–545. doi:10.1211/0022357022944
54. Korkina LG, Mikhal'chik E, Suprun MV, Pastore S, Dal Toso R. Molecular mechanisms underlying wound healing and anti-inflammatory properties of naturally occurring biotechnologically produced phenylpropanoid glycosides. *Cell Mol Biol (Noisy-Le-Grand)*. 2007;53:84–91.
55. Verma S, Singh A, Mishra A. Gallic acid: molecular rival of cancer. *Environ Toxicol Pharmacol*. 2013;35:473–485. doi:10.1016/j.etap.2013.02.011
56. Kapoor M, Howard R, Hall I, Appleton I. Effects of epicatechin gallate on wound healing and scar formation in a full thickness incisional wound healing model in rats. *Am J Pathol*. 2004;165:299–307. doi:10.1016/S0002-9440(10)63297-X
57. Yang DJ, Moh SH, Son DH, et al. Gallic acid promotes wound healing in normal and hyperglucidic conditions. *Molecules*. 2016;21:899. doi:10.3390/molecules21070899
58. Donà M, Dell'Aica I, Calabrese F, et al. Neutrophil restraint by green tea: inhibition of inflammation, associated angiogenesis, and pulmonary fibrosis. *J Immunol*. 2003;170:4335–4341. doi:10.4049/jimmunol.170.8.4335
59. Yen GC, Chen HY. Scavenging effect of various tea extracts on superoxide derived from the metabolism of mutagens. *Biosci Biotechnol Biochem*. 1998;62:9, 1768–1770. doi:10.1271/bbb.62.1768
60. Caturla N, Vera-Samper E, Villalaı´n J, Mateo CR, Micol V. The relationship between the antioxidant and the antibacterial properties of galloylated catechins and the structure of phospholipid model membranes. *Free Rad Biol Med*. 2003;34:648–662. doi:10.1016/S0891-5849(02)01366-7
61. Li CW, Wang Q, Li J, et al. Silver nanoparticles/chitosan oligosaccharide/poly (vinyl alcohol) nanofiber promotes wound healing by activating TGFβ1/Smad signaling pathway. *Int J Nanomedicine*. 2016;11:373–386. doi:10.2147/IJN.S91975
62. Gurunathan S, Lee KJ, Kalishwaralal K, Sheikpranbabu S, Vaidyanathan R, Eom SH. Antiangiogenic properties of silver nanoparticles. *Biomaterials*. 2009;30:6341–6350. doi:10.1016/j.biomaterials.2009.08.008
63. Park EJ, Pezzuto JM. The pharmacology of resveratrol in animals and humans. *Biochim Biophys Acta*. 2015;1852:1071–1113. doi:10.1016/j.bbadis.2015.01.014
64. Wu H, He L, Shi J, et al. Resveratrol inhibits VEGF-induced angiogenesis in human endothelial cells associated with suppression of aerobic glycolysis via modulation of PKM2 nuclear translocation. *Clin Exp Pharmacol Physiol*. 2018;45:1265–1273. doi:10.1111/1440-1681.13017
65. Lee B, Moon SK. Resveratrol inhibits TNF-alpha-induced proliferation and matrix metalloproteinase expression in human vascular smooth muscle cells. *J Nutr*. 2005;135:2767–2773. doi:10.1093/jn/135.12.2767
66. Ikeda K, Torigoe T, Matsumoto Y, Fujita T, Sato N, Yotsuyanagi T. Resveratrol inhibits fibrogenesis and induces apoptosis in keloid fibroblasts. *Wound Repair Regen*. 2013;21:616–623. doi:10.1111/wrr.12062
67. Ji Q, Liu X, Han Z, et al. Resveratrol suppresses epithelial-to-mesenchymal transition in colorectal cancer through TGF-β1/Smads signaling pathway mediated Snail/E-cadherin expr ession. *BMC Cancer*. 2015;15:97. doi:10.1186/s12885-015-1119-y
68. Chan CM, Chang HH, Wang VC, Huang CL, Hung CF. Inhibitory effects of resveratrol on PDGF-BB-induced retinal pigment epithelial cell migration via PDGFRβ, PI3K/Akt and MAPK pathways. *PLoS One*. 2013;8(2):e56819. doi:10.1371/journal.pone.0056819
69. Porter LJ. Flavans and proanthocyanidins. In: Harborne JB, editor. *The Flavonoids: Advances in Research Since 1986*. London: Chapman & Hall; 1994:23–55.

70. Stoupi S, Williamson G, Viton F, et al. In vivo bioavailability, absorption, excretion, and pharmacokinetics of [14C] proscyanidin B_2 in male rats. *Drug Metab Dispos*. 2010;38:287–291. doi:10.1124/dmd.109.030304
71. Tian Y, Yang C, Yao Q, et al. Procyanidin B2 activates PPARγ to induce M2 polarization in mouse macrophages. *Front Immunol*. 2019;10:1895. doi:10.3389/fimmu.2019.01895
72. Takahashi T, Kamiya T, Hasegawa A, Yokoo Y. Procyanidin oligomers selectively and intensively promote proliferation of mouse hair epithelial cells in vitro and activate hair follicle growth in vivo. *J Invest Dermatol*. 1999;112:310–316. doi:10.1046/j.1523-1747.1999.00532.x